

## Fission of doubly even actinide nuclei induced by direct reactions\*

B. B. Back and Ole Hansen

*Los Alamos Scientific Laboratory, University of California, Los Alamos, New Mexico 87544,  
and The Niels Bohr Institute, University of Copenhagen, Copenhagen, Denmark*

H. C. Britt and J. D. Garrett<sup>†</sup>

*Los Alamos Scientific Laboratory, University of California, Los Alamos, New Mexico 87544  
(Received 5 December 1973)*

Fission probability distributions have been measured by  $(t, pf)$ ,  $(t, \alpha f)$ ,  $(t, t'f)$ ,  $(p, p'f)$ ,  $(^3\text{He}, df)$ , and  $(^3\text{He}, \alpha f)$  reactions with bombarding energies of 15, 16, 20, 22.5, 24, and 24 MeV, respectively. Using targets of  $^{230,232,234}\text{Th}$ ,  $^{231}\text{Pa}$ ,  $^{234,236,238}\text{U}$ ,  $^{237}\text{Np}$ ,  $^{240,242}\text{Pu}$ ,  $^{243}\text{Am}$ , and  $^{248}\text{Cm}$  the fission decay of  $^{230,232,234}\text{Th}$ ,  $^{232,236,238,240}\text{U}$ ,  $^{238,242,244}\text{Pu}$ , and  $^{244,248,250}\text{Cm}$  was studied. Subbarrier vibrational resonances were observed for  $^{234}\text{Th}$ ,  $^{236,238,240}\text{U}$ ,  $^{242}\text{Pu}$ , and  $^{250}\text{Cm}$ . The results are analyzed with a statistical model which involves resonant penetration of the double-humped fission barrier. Estimates of the heights and curvature of the two peaks in the fission barrier are obtained for Th, U, Pu, and Cm isotopes and these values are compared with various theoretical calculations.

NUCLEAR REACTIONS FISSON measured fission probabilities,  $E^* \leq 7.5$  MeV for  $^{230,232,234}\text{Th}$ ,  $^{232,236,238,240}\text{U}$ ,  $^{238,242,244}\text{Pu}$ ,  $^{244,248,250}\text{Cm}$  using  $(t, pf)$ ,  $(t, \alpha f)$ ,  $(t, t'f)$ ,  $(p, p'f)$ ,  $(^3\text{He}, df)$ ,  $(^3\text{He}, \alpha f)$  reactions; deduced heights and curvatures for the double-peaked fission barrier for each case.

### 1. INTRODUCTION

In recent years studies of the fission process have been strongly influenced by the discovery of a secondary minimum in the fission barrier<sup>1-4</sup> and by the subsequent theoretical studies<sup>5-10</sup> which have shown that the inclusion of single-particle shell corrections to a smooth liquid-drop barrier leads to the prediction of a two-peaked fission barrier in the actinide region. One experimental method that has been used<sup>11-15</sup> to study fission-barrier properties consists in exciting a nucleus to energies near the fission threshold through a direct reaction and then measuring the probability that the nucleus will deexcite by fission. This experimental method has two distinct advantages over the more conventional neutron-induced fission studies. Firstly, the region of excitation energy below the neutron binding energy can be studied and, secondly, a wider range of fissioning nuclei can be reached using available targets.

The direct-reaction induced-fission experiments measure the branching of fission relative to other decay modes at energies near the top of the barrier. If one of the peaks of the fission barrier is much higher than the other, then the experiments give only information on the height and curvature of the highest peak. However, if the two peaks are of comparable heights, then in some cases resonances are observed in the fission probability at energies near the top of the lowest peak. Resonance structures have previously been observed<sup>11-15</sup>

in the fission probability for several doubly even isotopes of uranium and plutonium. These resonances are identified with vibrational excitations in the second well, as illustrated in Fig. 1.

In the analysis of previous results<sup>14,16</sup> it was discovered that the observed resonances were significantly broader than expected from the penetrabilities of the two peaks. This additional broadening was attributed to a coupling (or damping) in the second well of the vibrational states with the more numerous compound states of the same total energy. For odd- $A$  and doubly odd nuclei this damping would be expected to be larger than in doubly even isotopes because of the greater density of compound states near the top of the barrier encountered in these cases. This prediction is consistent with results for odd nuclei which generally do not show resonant structure indicating that the damping width is larger than the average spacing of fission transition states.

A further difference between the odd and the doubly even nuclei is that the fission thresholds for doubly even nuclei are generally below the neutron binding energy so that only fission and  $\gamma$  decay compete, whereas for many odd nuclei neutron decay is also important near threshold.

The aim of the present experiments was to investigate the fission barrier systematics over the actinide region. To do this we have measured fission probability distributions using a variety of reactions and targets leading to doubly even, odd- $A$ , and doubly odd nuclei. Because of fundamental

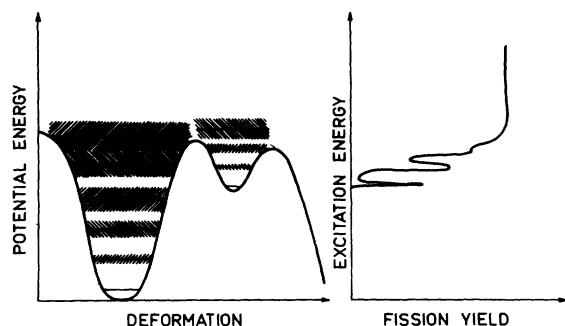


FIG. 1. Schematic illustration of the yield from fission through a two-peaked barrier. The horizontal lines indicate positions of vibrational resonances in the first and second wells and the cross-hatching schematically indicates their width.

differences in the analyses and interpretations, the data naturally split into two categories; the doubly even nuclei where resonance behavior often is observed, and the remaining odd- $A$  and doubly odd nuclei. In this paper we will be concerned with even-even nuclei only, whereas data and analysis of the odd- $A$  and odd-odd nuclei will be presented in subsequent publications.<sup>17</sup> Brief reports of some of these experimental results have also been published previously.<sup>18-21</sup>

## 2. EXPERIMENTAL PROCEDURES AND DATA REDUCTION

### A. Experimental procedures

The beams were provided by the Los Alamos tandem and three-stage Van de Graaff accelerator facility. The  $(t, pf)$  and  $(t, \alpha f)$  experiments were studied at 15- and 16-MeV bombarding energy, respectively, while the  ${}^3\text{He}$ -induced fission was studied at 24 MeV. The  ${}^{248}\text{Cm}(p, p'f)$  reaction utilized 22.5-MeV protons from the three-stage mode of acceleration and the  $(t, t'f)$  experiment on the same target was performed at 20 MeV.

The bombarding energies were not very critical; they represent compromises between the geometry of the detection system, reaction cross sections, and attempts to minimize the ratio of accidental to coincidence events. The first and last items favored a light-particle detection system near  $90^\circ$ , while the middle requirement would in some cases lead to smaller reaction angles. The use of bombarding energies just above the Coulomb barrier (15-16-MeV tritons in and  $\sim 12$ -MeV protons out, for example) lead to light-particle angular distributions that are quite flat and with about equal intensities predicted at  $90^\circ$  for angular momentum transfers from 0 to 6 in the  $(t, p)$  process. When

the bombarding energy in the  $(t, pf)$  process was raised to 20 MeV, the  $(t, p)$  yield at  $90^\circ$  fell drastically rendering data taking impractical. As a general rule of thumb, the counting rates were best when both the in and outgoing particles had energies a few MeV over the Coulomb barrier. This leads to the 15-16-MeV triton energies for  $(t, pf)$  and  $(t, \alpha f)$  reactions, and to  $\sim 27$  MeV for the  ${}^3\text{He}$ -induced reactions, which was not available and, therefore, bombarding energies of 24 MeV were used for these reactions. Negative  $Q$ -value direct reactions were difficult requiring bombarding energies far above the Coulomb barrier; thus we had no success in a search for  $(p, df)$  reactions and the  $(p, p'f)$  process was only used in one case.

The targets (except  ${}^{248}\text{Cm}$ ) were made by the vacuum evaporation of the isotope onto  $\sim 50$ - $\mu\text{g}/\text{cm}^2$  carbon backings. Thicknesses were typically  $\sim 200$   $\mu\text{g}/\text{cm}^2$  and enrichments were  $>98\%$  except for  ${}^{230}\text{Th}$  where it was  $\sim 90\%$  with a 10% impurity of  ${}^{232}\text{Th}$ . In the analysis of data taken with this target, a correction was made for fission induced by reactions on the  ${}^{232}\text{Th}$  target impurity. The  ${}^{248}\text{Cm}$  target was made at the Argonne National Laboratory by collecting the separated isotope directly on the target backing. The purity was  $\sim 99\%$  with  $\sim 80$ - $\mu\text{g}/\text{cm}^2$  thickness of the Cm deposit.

The detection system is illustrated in Fig. 2. The beam was focused through a 4-mm hole in the annular fission detector to strike the target at a  $\sim 45^\circ$  angle. The beam was stopped in a Faraday cup  $\sim 2$  m behind the target. The fission fragments were registered in the annular detector covering laboratory angles from  $\sim 120$  to  $\sim 175^\circ$  with respect to the beam axis. The light-ion reaction products were detected in a  $\Delta E$ - $E$  telescope situated at  $\sim 90^\circ$  lab angle. The  $\Delta E$  detectors were from 100- to 300- $\mu\text{m}$ -thick fully depleted Si detectors, while the  $E$  counters were  $\sim 2$ -mm-thick Si detectors. The upper limit on the useful solid angle ( $\sim 25$  msr) was determined by the kinematical broadening of lines from the light-target impurities ( ${}^{12}\text{C}$  and  ${}^{16}\text{O}$ ) which tend to obscure important parts of the singles spectra. This geometry corresponds to recoil angles near  $30^\circ$  for the final nucleus, yielding an-

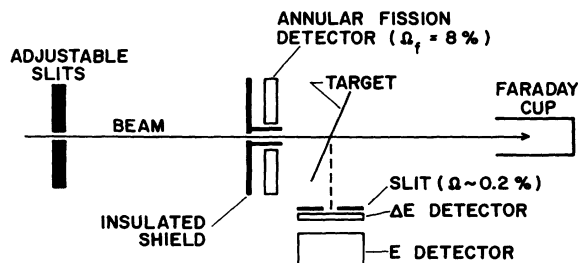


FIG. 2. Schematic diagram of the experimental setup.

gles of acceptance from 180 to 120° from the dominant recoil direction for the detected fission fragments.

A simplified version of the electronics arrangement is given in Fig. 3. The analog signals are gated into separate analog-to-digital converters (ADCs); the gate pulse was generated either by a (slow) triple coincidence of signals from the  $\Delta E$ ,  $E$ , and fission counters or by the single occurrence of an  $E$  pulse (usually scaled down by a factor of 100). The latter event would not be accompanied by any time pulse and would therefore be registered as a singles pulse. The ADCs were read out by the SDS930 on-line computer system and each event was recorded on magnetic tape for later off-line analysis. The time resolution was typically 2–3 ns.

On-line analysis also was performed. The mass of the light ejectile was first determined from the  $E + \Delta E$  and  $\Delta E$  signals; if this mass fell within a selected window, the time signal was looked up. If the time signal fell within the window selected for "true coincidences" the event was stored and displayed on the data screen as such. A window for "accidental coincidences" was also selected in the time spectrum and an "accidental" spectrum was stored and displayed. If there was no time pulse accompanying the gated event, it was stored as a singles event. Thus the on-line computer could currently display five spectra; a mass spectrum (with one window allowed), a time spectrum (two windows), a "true," an "accidental," and a "singles" spectrum. This was found ample for on-line control of the data acquisition. The results shown below were obtained by replaying the tape after the experiment, optimizing the window settings, and in some cases analyzing for different mass windows.

The correction for accidental coincidence events was usually made by appropriately scaling the singles spectrum, since most often the accidental coincidence spectra themselves had too poor statistics to provide an accurate correction. Counting rates in the fission counter usually had to be kept below 20 000 counts per second to ensure a favorable true to accidental ratio; this in most cases

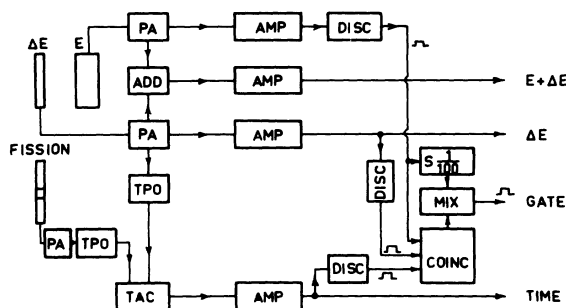


FIG. 3. Schematic diagram of the electronics configuration. S represents a scale-down circuit which could be set at values from 1 to 1/1000 in factors of 1/10. PA, TPO, and TAC represent preamplifiers, time-pickoff fast discriminators, and a time-to-amplitude converter, respectively.

corresponded to beam current of 30–60 nA. Typically it took 24–48 hours to collect the data corresponding to one target and projectile.

An energy calibration was obtained with an estimated accuracy of  $\pm 50$  keV by recording spectra from the appropriate reaction on a  $^{208}\text{Pb}$  target using the established ground-state  $Q$  values and excitation energies. Table I lists the known excitations in nuclei near  $^{208}\text{Pb}$  which were used for the calibration of the various reactions.<sup>22–25</sup> Ground-state masses were taken from Ref. 26 except the  $^{250}\text{Cm}$  g.s. mass which was measured.<sup>19</sup>

The solid angle  $\Omega$ , of the fission detector is essential for extracting the fission probability and it was measured by inserting an  $\alpha$  source of approximately the same size and at the same position as the beam spot on the target. The solid angle of the fission detector was established by measuring the counting rate in the fission detector relative to the counting rate in a detector with known solid angle. The accuracy of such a measurement is determined by how close the position of the  $\alpha$  source is to the actual position of the beam spot during the run. The precision of this measurement is estimated to be better than  $\sim 10\%$  and this introduces an uncertainty of similar magnitude in the resulting fission probabilities.

TABLE I. Energy levels in nuclei near  $^{208}\text{Pb}$  used for the energy calibration.

| Reaction           | Product nucleus   | Energy levels (keV)                     | Ref. |
|--------------------|-------------------|---|------|
| $(p, p')$          | $^{208}\text{Pb}$ | 2615, 3198, 4070, 4305                  | 22   |
| $(t, p)$           | $^{210}\text{Pb}$ | 804, 1099, 1197, 1281, 2222, 2522, 2706 | 23   |
| $(t, \alpha)$      | $^{207}\text{Tl}$ | 350, 1341, 1674                         | 24   |
| $(^3\text{He}, d)$ | $^{208}\text{Bi}$ | 892, 1601, 2591, 2814, 3108, 3624, 4406 | 25   |

## B. Data reduction

The fission probability is defined as

$$P_f = \frac{4\pi}{2\Omega_f} \frac{N_{\text{coinc}}}{N_{\text{singl}}} \quad (1)$$

The factor of 2 in the denominator is a result of the possibility of detecting either of the two fission fragments.

The relatively high counting rates give rise to an accidental contribution in the coincidence spectrum. A correction is made by normalizing the singles spectrum and subtracting it from the coincidence spectrum. In some cases the singles spec-

trum from the heavy element is somewhat obscured by strong and broad peaks stemming from  $^{12}\text{C}$  and  $^{16}\text{O}$  impurities in the target. Extrapolation under these peaks is necessary and introduces another source of uncertainty in the fission probability in these energy intervals. Another possible error source is due to the neglect of the angular correlation of the fission fragments with respect to the recoil angle. Such correlation effects were neglected in the extraction of the fission probabilities. The errors introduced may be estimated from the geometry of the present experiments and from comparisons to previous data<sup>27</sup> where the angular correlations of the fragments were measured.

Allowing for the possible systematic uncertainties the absolute accuracy of the measured fission probabilities is estimated to be better than ~20%.

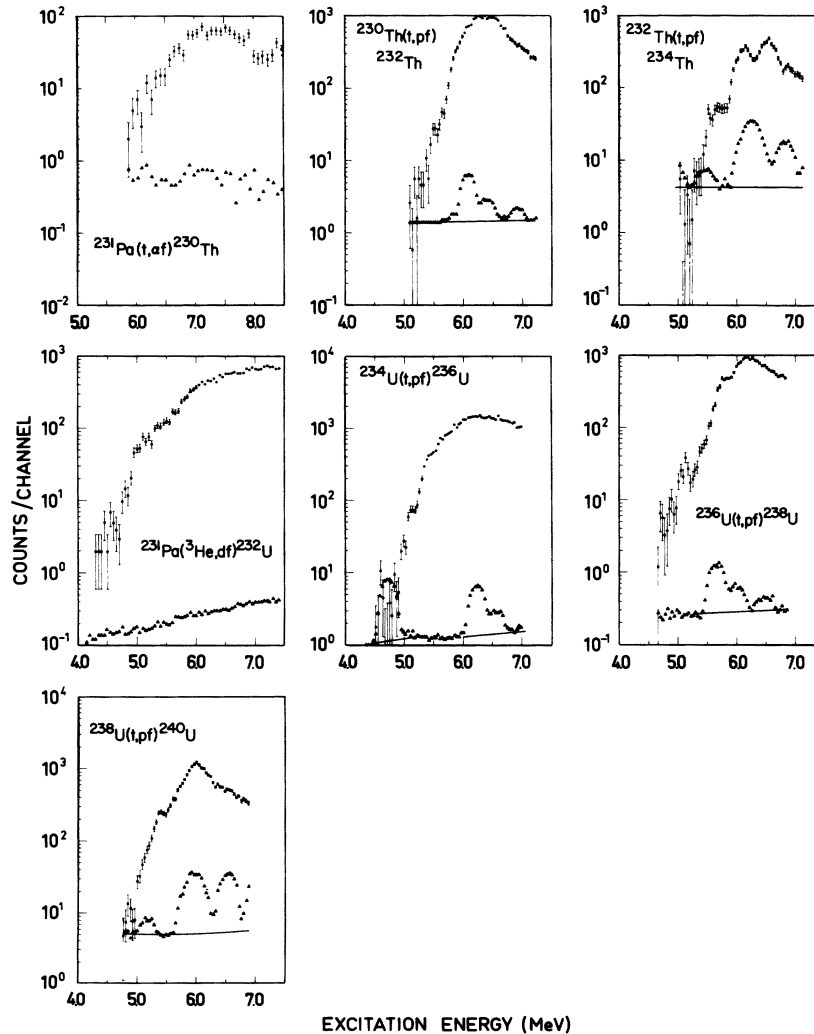


FIG. 4. Measured coincidence (circles) and singles (triangles) spectra for reactions leading to thorium and uranium nuclei. Solid lines indicate interpolated singles cross sections for the heavy-target element. Singles spectra have been normalized to the level of the accidental contributions in the coincidence spectrum.

## 3. EXPERIMENTAL RESULTS

The experimental data are shown in Figs. 4 and 5 for fissioning nuclei of Th, U, Pu, and Cm. Each figure identifies the appropriate reaction, shows the number of coincident light-particle events corrected for accidental events vs excitation energy (black circles with error bars), and shows the accidental spectrum (filled triangles) drawn to scale. The broad peaks in the accidental spectra are from reactions on  $^{12}\text{C}$  and  $^{16}\text{O}$ . The angle for detection of light ejectiles was chosen in order to shift these impurity peaks away from the threshold region where they could obscure fission resonances.

Table II lists the position of resonances and the

maximum fission probability which in most cases occurs at the neutron binding energy  $B_n$ . It is seen that resonance structure occurs for one Th isotope and systematically through the five doubly even U isotopes. Only two pronounced resonances are observed in the four Pu isotopes and finally there is just one isotope with resonance structure among the three Cm isotopes investigated. This demonstrates that the conditions for observing resonances are best fulfilled in the region  $Z \approx 92-94$  and  $N=146-148$ .

From the general trend of the slopes of the fission probabilities in the threshold region, it appears that the curves become less steep when going from Th to Cm nuclei. It also is observed that the slope increases going from neutron-deficient to neutron-rich isotopes of the same element.

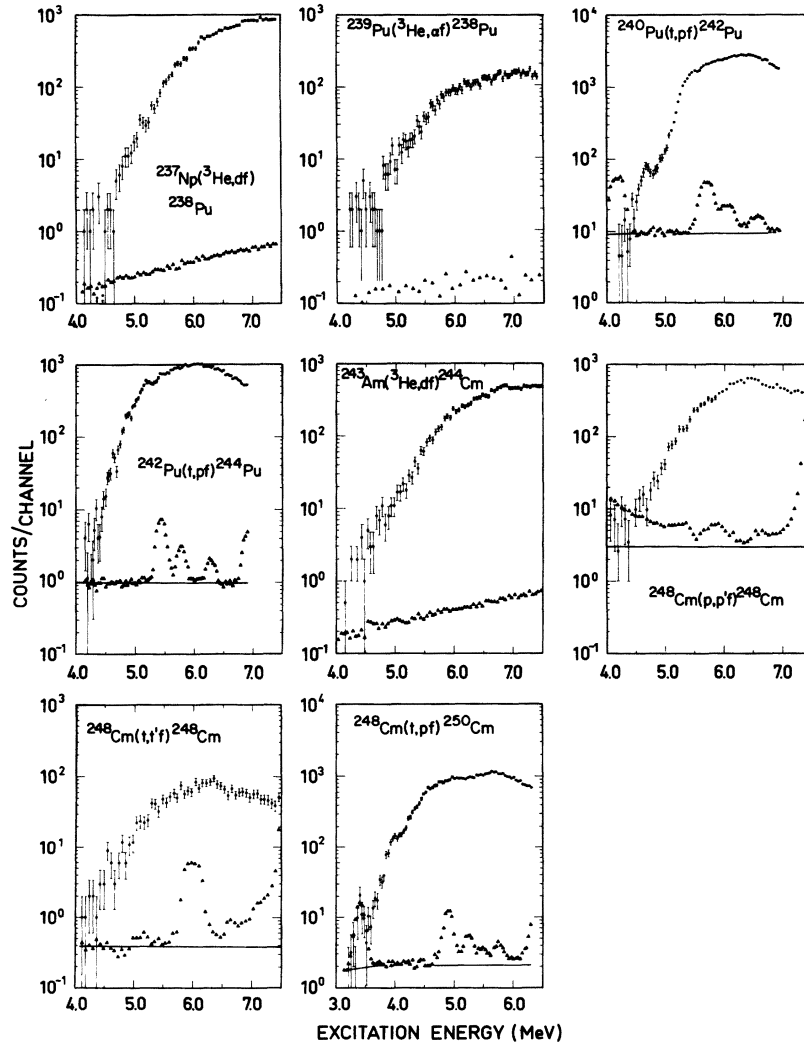


FIG. 5. Measured coincidence (circles) and singles (triangles) spectra for reactions leading to plutonium and curium nuclei. Solid lines indicate interpolated singles cross sections for the heavy-target element. Singles spectra have been normalized to the level of the accidental contributions in the coincidence spectrum.

We take the steeper curves to indicate that the outer fission barrier, which is usually broader than the inner one, dominates the threshold region, i.e. is higher than the inner barrier. The less steep slopes in the fission probabilities conversely show that the inner more penetrable barrier is the higher, and hence is decisive for the threshold region.

In some cases like  $^{234}\text{Th}$ ,  $^{234}\text{U}$ ,  $^{238}\text{U}$ , and  $^{240}\text{U}$  the neutron binding energy  $B_n$  is relatively close to the fission threshold and the maximum fission probability seems to be very strongly connected to the position of  $B_n$ . In these cases the neutron emission competes favorably with the fission decay starting at the neutron binding energy. In the other cases where the fission probability has saturated before reaching the neutron binding energy, the effect of the neutron emission is not nearly so drastic.

In some cases it is possible to compare to earlier work<sup>27</sup> (Fig. 6) and generally the two sets of measurements agree well except for an energy shift of  $\sim 100$  keV, which probably is a result of uncertainties in the energy calibration of Ref. 27. The previous results were obtained from an integration over a measured angular correlation for the fission fragments. The agreement observed between the two results indicates that the present experiments with a single large fission detector give an accurate measurement of the absolute value of the fission probability. The small differences in shape are most probably due to the better energy resolution and the ability to measure smaller fission probabilities in the present experiments.

#### 4. THEORY

##### A. General assumptions of model

In the following we discuss the qualitative aspects of both the calculation of the formation process [i.e., relative excitation probabilities  $\alpha(J\pi)$  for exciting states with a particular spin and parity in the direct reactions] and the decay process (i.e., calculation of  $\Gamma_f/\Gamma_\gamma$  as a function of energy, spin, and parity). In the next section the formal aspects of the theoretical model used to reproduce the experimental results will be outlined. In this theoretical model the standard "compound-nucleus" assumption that the formation and decay of the residual nucleus are independent, will be used.

##### 1. Formation process

Since we are interested in the fission probability and not in absolute fission cross sections, only relative probabilities  $\alpha(EJ\pi)$  for exciting states with excitation energy  $E$  and spin and parity  $J\pi$  in the residual nucleus are needed. The population probability  $\alpha(EJ\pi)$  was obtained from direct-reaction calculations employing the distorted-wave Born approximation (DWBA) with currently accepted parameters and empirical level-density estimates as described in Sec. 4 B 2. Results of the DWBA calculations are shown in Fig. 7 for the  $(d, p)$ ,  $(^3\text{He}, d)$ , and  $(t, p)$  reactions. The  $(d, p)$  and  $(^3\text{He}, d)$  results were obtained with the code DWUCK<sup>28</sup> while the  $(t, p)$  results were taken from previous calculations<sup>12,27</sup> which assumed that a dineutron coupled to spin 0 and isospin 1 was transferred to the target.

TABLE II. Summary of reactions studied.

| Compound nucleus  | Reaction         | Target            | Energy (MeV) | Angle (deg) | Resolution (FWHM) (keV) | Target spin     | $E_{\text{resonance}}$ (MeV) | $P_{f\text{max}}$ | Ref.    |
|-------------------|------------------|-------------------|--------------|-------------|-------------------------|-----------------|------------------------------|-------------------|---------|
| $^{230}\text{Th}$ | $t, \alpha$      | $^{231}\text{Pa}$ | 16.0         | 90          | 140                     | $\frac{3}{2}^-$ |                              | $\sim 0.24$       | Present |
| $^{232}\text{Th}$ | $t, p$           | $^{230}\text{Th}$ | 15.0         | 90          | 60                      | $0^+$           | (5.5)                        | 0.33              | Present |
| $^{234}\text{Th}$ | $t, p$           | $^{232}\text{Th}$ | 15.0         | 70          | 75                      | $0^+$           | 5.5, 5.8                     | 0.09              | Present |
| $^{232}\text{U}$  | $^3\text{He}, d$ | $^{231}\text{Pa}$ | 24.0         | 90          | 95                      | $\frac{3}{2}^-$ |                              | 0.75              | Present |
| $^{234}\text{U}$  | $d, p$           | $^{233}\text{U}$  | 13.0         | 140         | $\sim 65$               | $\frac{3}{2}^+$ | 5.0, (5.5)                   | 0.45              | a       |
| $^{236}\text{U}$  | $t, p$           | $^{234}\text{U}$  | 15.0         | 90          | 75                      | $0^+$           | 5.1                          | 0.80              | Present |
| $^{238}\text{U}$  | $t, p$           | $^{236}\text{U}$  | 15.0         | 90          | 75                      | $0^+$           | 5.15, 5.8                    | 0.40              | Present |
| $^{240}\text{U}$  | $t, p$           | $^{238}\text{U}$  | 15.0         | 70          | 75                      | $0^+$           | 5.4                          | 0.30              | Present |
| $^{238}\text{Pu}$ | $^3\text{He}, d$ | $^{237}\text{Np}$ | 24.0         | 90          | 105                     | $\frac{3}{2}^+$ | (5.1)                        | 0.82              | Present |
| $^{240}\text{Pu}$ | $t, p$           | $^{238}\text{Pu}$ | 15.0         | 115         | $\sim 110$              | $0^+$           | (4.5), 5.0                   | 0.60              | b       |
| $^{242}\text{Pu}$ | $t, p$           | $^{240}\text{Pu}$ | 15.0         | 80          | 75                      | $0^+$           | 4.65                         | 0.60              | Present |
| $^{244}\text{Pu}$ | $t, p$           | $^{242}\text{Pu}$ | 15.0         | 90          | 65                      | $0^+$           | (4.6)                        | 0.64              | Present |
| $^{244}\text{Cm}$ | $^3\text{He}, d$ | $^{243}\text{Am}$ | 24.0         | 90          | 85                      | $\frac{3}{2}^-$ |                              | 0.52              | Present |
| $^{248}\text{Cm}$ | $p, p'$          | $^{248}\text{Cm}$ | 22.5         | 90          | 95                      | $0^+$           |                              | 0.45              | Present |
| $^{250}\text{Cm}$ | $t, p$           | $^{248}\text{Cm}$ | 15.0         | 90          | 75                      | $0^+$           | (3.4), 4.0                   | 0.50              | Present |

<sup>a</sup> Back *et al.*, Ref. 31.

<sup>b</sup> Cramer and Britt, Ref. 27.

The transition-state spectra involved in the fission decay include rotational bands with many spin states spaced close together, so details of the shape of the  $\alpha(EJ\pi)$  distribution should not be crucial. Calculations were made which show that the predicted fission probabilities  $P_f(E)$  are indeed quite insensitive to the assumed  $\alpha(EJ\pi)$  distributions.

## 2. Decay process

We assume that a nucleus excited to a particular state can either decay by fission with statistical probabilities through all transition states or by  $\gamma$ -ray emission. The energy region above the neutron-emission threshold will not be considered. Since the experimental results in some cases show resonance structure, the transmission through the two peaks of the fission barrier must be treated in a coherent manner. This is done by calculating analytically the penetrability through a two-peaked fission barrier which is composed of three smoothly joined parabolic sections.<sup>29,30,14</sup> Thus, the relevant parameters are  $E_A$ ,  $\hbar\omega_A$ ,  $E_{II}$ ,  $\hbar\omega_{II}$ ,  $E_B$ , and  $\hbar\omega_B$  where all energies are measured relative to the ground-state energy (see Fig. 8).

It has been shown<sup>14,31,32</sup> that the observed sub-barrier fission resonances in some cases are considerably broader than those calculated from pure resonant penetration of the barrier. Therefore, broadening due to damping of the fission resonances in the second well into underlying states with the same total energy must be included in the model. The strength assumed for this damping

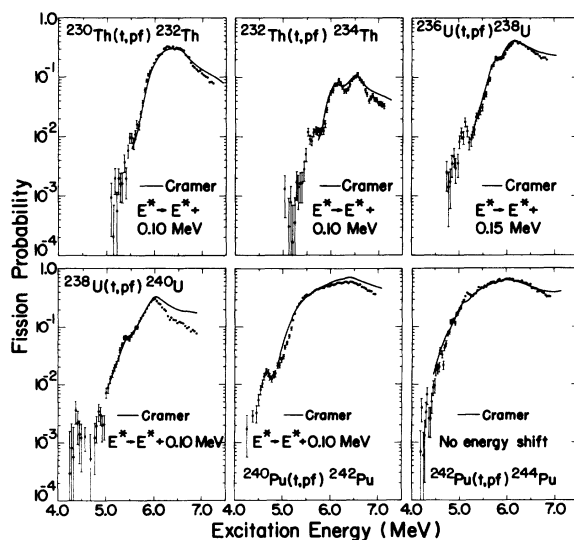


FIG. 6. Fission-probability distributions for several cases compared to previous results from Cramer (Ref 27). The energy scales for the results of Ref. 27 have been shifted as indicated.

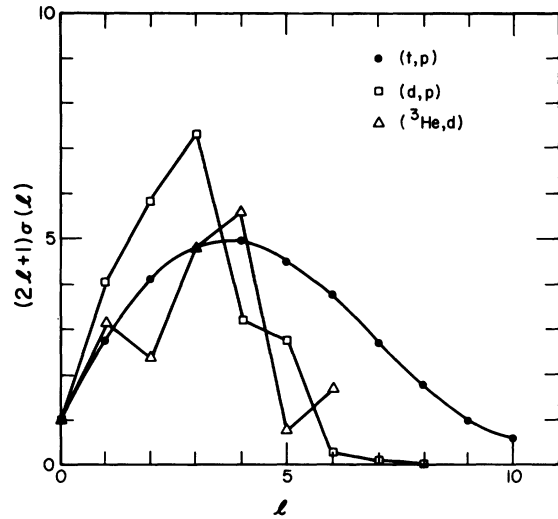


FIG. 7. Differential cross sections at  $90^\circ$  as a function of orbital angular momentum transfer  $l$  for the  $(t,p)$ ,  $(d,p)$ , and  ${}^3\text{He},d$  reactions normalized to 1.0 for  $l=0$ .

introduces another parameter into the model. If there is significant mixing in the second well between the fission resonance states and other compound states, then it may also be possible for the nucleus to change from one internal configuration to another and this may possibly alter the value of  $K$  (the projection of the spin on the symmetry axis).

The most general model consistent with the above requirements would involve the calculation of penetrabilities for all possible transition states with each state having its own set of six barrier parameters. In addition, mixing in the second well should be included. This approach, however, introduces too many parameters and some simplifying approximations must be made in order to render the problem tractable.

The model adopted for the analysis of the present

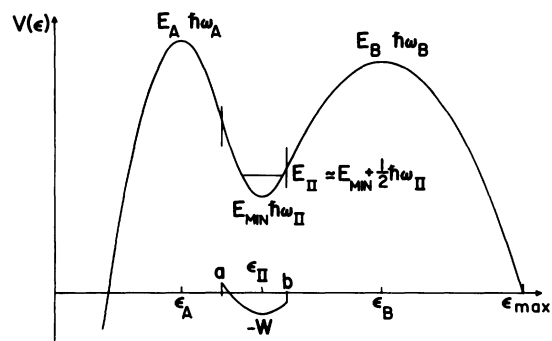


FIG. 8. A schematic illustration of the parametrization used for the one-dimensional fission barrier. All energies are measured relative to the energy of the ground state.

experimental results incorporates the assumption that the motion in the fission degree of freedom is completely decoupled from all other modes of excitation except for the damping in the second well. In this limit there is only one shape of the fission barrier valid for all transition states and excitation of internal degrees of freedom simply reduces the energy available in the fission mode. If this assumption is to hold true, it is required that the energies associated with the various internal excitations be independent of deformation in the region of the fission barrier. This assumption is appropriate for small regions of deformation near a saddle point, but its validity is questionable for the extended deformation region covering the two peaks of the fission barrier.

In the region of excitation energy below the pairing gap ( $\sim 1.5$  MeV) for a doubly even nucleus the possible internal excitations of the nucleus at the saddle-point deformations consist of only a few vibrational excitations with accompanying rotational bands. The lowest-lying vibrational bands should be the  $K=0^+$  (ground-state band),  $K=2^+$  ( $\gamma$ -vibrational band), and the negative-parity octupole vibrations with  $K=0^-$ ,  $1^-$ , and possibly  $2^-$ .

Recent theoretical calculations<sup>7,33-38</sup> have indicated that in some cases the spectrum of transition states at the two saddle points may be quite different in contradiction to the assumption that we can decouple the fission motion from the other internal degrees of freedom. In particular for most nuclei of interest here the second saddle point is unstable toward octupole deformations that would reduce the internal energy associated with  $K=0^-$ ,  $1^-$ , and  $2^-$  bands while the first saddle point for isotopes of plutonium and heavier nuclei may be unstable toward  $\gamma$  deformations which would lower the energy of the  $K=2^+$  band in that region. These effects would lead to qualitatively different shapes for the fission barriers associated with  $K=0^+$ ,  $K=2^+$ , and the negative-parity bands.

Test calculations with the current model have shown that, except for details of the resonant penetrations, the  $P_f(E)$  distributions are reasonably well reproduced by putting the  $K=0^-$  and  $K=2^+$  excitations at the average energy at the two peaks. Thus, by reproducing the fission probability distributions we expect to get reasonably good estimates of the heights and curvatures of the two peaks in the fission barrier, but the estimates for the energies associated with the various vibrations could be misleading. However, the different shapes for barriers associated with different transition states can have a much larger effect on the calculation of the fission-fragment angular correlations. This subject is discussed in more detail in Appendix I.

Another serious approximation used in the present model is that we effectively assume strong coupling between the levels in well I and well II when the damping of the fission motion into compound states in well II is considered. This approximation considerably simplifies the calculations, but it may lead to some systematic errors in the estimates for  $\hbar\omega_A$ ,  $\hbar\omega_B$ , and the strength assumed for the damping in the second well. A detailed discussion of these effects is given in Appendix II.

## B. Details of model

### 1. General

The theoretical description of the calculation of fission-probability distributions for the ( $t, pf$ ) and ( $d, pf$ ) reactions has been published previously<sup>12, 16, 31</sup> and, therefore, will not be considered in detail in this paper. The extensions of the model to other reactions are straightforward and are therefore neither dealt with in detail. In general, the fission probability can be written as

$$P_f(E) = \sum_{J\pi} \left( \alpha(EJ\pi) \left\langle \frac{\Gamma_f(EJ\pi)}{\Gamma_f(EJ\pi) + \Gamma_\gamma(EJ\pi)} \right\rangle \right), \quad (2)$$

where the average is taken over many levels in the fissioning nucleus. The quantity  $\alpha(EJ\pi)$  denotes the average probability of populating compound levels with spin and parity  $J\pi$  at the excitation energy  $E$ .  $\Gamma_f$  and  $\Gamma_\gamma$  are the partial widths for fission and  $\gamma$  decay, respectively. The fission probabilities were calculated using the approximate relationship<sup>12, 16, 31</sup>

$$P_f(E) = \sum_{J\pi} \left( \alpha(EJ\pi) \frac{\langle \Gamma_f(EJ\pi) \rangle}{\langle \Gamma_f(EJ\pi) \rangle + \langle \Gamma_\gamma(EJ\pi) \rangle} F \right), \quad (3)$$

where  $F$  is a calculated factor<sup>31</sup> that takes into account the reduction in  $P_f(E)$  due to the statistical distribution of individual  $\Gamma_f(EJ\pi)$  values about their mean.

### 2. Formation cross section

In the present analysis we have made fairly simple statistical assumptions for calculating the relative excitation probability  $\alpha(EJ\pi)$  of compound states of different spin and parity. In our treatment  $\alpha$  is independent of energy and is given by

$$\alpha(EJ\pi) = \alpha(J\pi) = N_0 \rho(J\pi) \sum_{j=|J-I_0|}^{J+I_0} \frac{\sigma(j\pi)}{(J+I_0) - |J-I_0| + 1}, \quad (4)$$

where  $N_0$  is a normalization constant determined by

$$\sum_{J\pi} \alpha(J\pi) = 1. \quad (5)$$

$J\pi$  designates the final-state spin reached in the direct reaction from the target state of spin  $I_0$ .  $j\pi$  is the transferred spin and parity.

$$\rho(J\pi) = \frac{1}{2}(2J+1) \exp\left(-\frac{(J+\frac{1}{2})^2}{2\sigma_j^2}\right) \quad (6)$$

is the statistical spin density and  $\sigma_j^2$  is the normal spin-cutoff factor while  $\sigma(j\pi)$  is the DWBA calculated transfer cross section. In the case of ( $t, pf$ ) on an even-even target we get

$$\alpha(J\pi) = N_0 \rho(J\pi) \sigma(L=J, \pi), \quad (7)$$

where

$$\sigma(J\pi) = \sigma[J=L, \pi=(-1)^L] \quad (8)$$

and  $L$  is the transferred angular momentum. This means that only natural-parity states are excited under the assumption that the two neutrons are transferred in a relative  $s$  motion.

### 3. Calculation of the fission width

The fission width is composed of contributions from decay through different fission channels  $\nu$  and can therefore be written as

$$\Gamma_f(EJ\pi) = \sum_{\nu} \Gamma_f^{\nu}(EJ\pi). \quad (9)$$

Using the standard Weisskopf formula we can relate the average partial-fission width through a single channel  $\nu$  with the transmission coefficient  $T_f$  and the average level spacing  $D$  by the formula

$$\langle \Gamma_f^{\nu}(EJ\pi) \rangle = \frac{D(EJ\pi)}{2\pi} T_f^{\nu}. \quad (10)$$

The transmission coefficient  $T_f$  through the fission barrier is calculated assuming a double-humped fission barrier with an intermediate minimum which gives rise to resonances at the positions of the quasibound states in the second well. In the calculation of  $T_f^{\nu}$  we approximate the shape of the barrier  $V(\epsilon)$  by three parabolic sections joined smoothly at the points  $a$  and  $b$  (see Fig. 8). The real part of the potential is described by six parameters, namely the heights and curvatures of the two peaks  $E_A$ ,  $\hbar\omega_A$ ,  $E_B$ , and  $\hbar\omega_B$  and the height  $E_{\min}$  and curvature  $\hbar\omega_{II}$  of the secondary minimum.

Analogous to the situation in the first well where the  $\beta$ -vibrational strength is damped into the underlying compound states, it is expected that similar couplings between the fission mode and the internal degrees of freedom will occur in the second well when the level density is large enough. In the model we have simulated this damping by absorbing out flux from the pure fission motion and redistributing it in internal excitations. This is done by adding to the real part of the potential a

negative imaginary part at the position of the second well.<sup>31</sup> The shape of the imaginary part is also a parabolic section with minimum value  $-W$  and a curvature determined by (see Fig. 8)

$$\text{Im}[V(a) + V(b)] = 0. \quad (11)$$

The strength of the imaginary potential  $-W$  is assumed to have a linear dependence on the excitation energy

$$-W(E) = -w[E - E_{\min} - \Delta_n - \Delta_p] - W_0. \quad (12)$$

The pairing gaps for neutrons and protons are denoted  $\Delta_n$  and  $\Delta_p$ , respectively. With this parametrization it is possible to solve the penetration problem by matching the analytical solutions to the Schrödinger equation<sup>29, 30</sup> (parabolic cylinder functions) at  $\epsilon = a$  and  $\epsilon = b$ . One finds that an incoming unity flux splits into three parts, namely a directly transmitted flux  $T_D$ , a reflected flux  $R$ , and finally an absorbed flux  $A$ , which satisfy the relation

$$1 = T_D + A + R. \quad (13)$$

The internal modes in the second well that have been excited through the absorbed flux  $A$  can decay in three ways, namely by  $\gamma$  emission, penetration of the first barrier, and by penetration of the second barrier which leads to fission. This latter part contributes to  $T_f^{\nu}$  and can be estimated as the absorbed flux  $A$  times a branching ratio

$$T_I = A \frac{P_B}{P_A + P_B}. \quad (14)$$

The total transmission coefficient is then

$$T_f = T_D + T_I. \quad (15)$$

The penetration factors  $P_A$  and  $P_B$  are calculated using a normal Hill-Wheeler formula<sup>39</sup>

$$P(E) = \left\{ 1 + \exp\left[\frac{2\pi}{\hbar\omega}(B_f - E)\right] \right\}^{-1}, \quad (16)$$

where  $B_f$  is the fission barrier and  $\hbar\omega$  the curvature.  $P_{\gamma}$  is negligible compared to these two quantities at the relevant energies and is therefore omitted in the calculation.

### 4. $K$ mixing in the second well

The excitation of internal degrees of freedom in the second well also makes it possible for the nucleus to change its  $K$  value (i.e., spin projection along the symmetry axis) during the time the energy is bound in internal motions.<sup>16</sup> This effect is referred to as  $K$  mixing and it has a fairly small effect on the resulting fission-probability distribution, but an appreciable effect on the angular correlations of the fission fragments (see

Appendix I). Formally we describe the  $K$ -mixing effect by adding the absorption from different transition states  $\nu$  irrespective of the associated  $K$  value into one quantity  $N_{\text{abs}}(EJ\pi)$  preserving the spin  $J$  and the parity  $\pi$

$$N_{\text{abs}}(EJ\pi) = \sum_{\nu} A^{\nu}(EJ\pi). \quad (17)$$

(To each  $\nu$  corresponds only one  $K$  value.) The final  $K$  distribution of the indirect flux is now determined by the transparencies of the outer barrier for various transition states  $\nu$  and consequently the associated  $K$  values<sup>16</sup>

$$T_{\Gamma}^{\nu}(EJ\pi) = N_{\text{abs}}(EJ\pi) \frac{P_B^{\nu}(EJ\pi)}{\sum_{\nu} [P_A^{\nu}(EJ\pi) + P_B^{\nu}(EJ\pi)]}. \quad (18)$$

In this formula the  $\gamma$  decay in the second well is disregarded. Thus, the partial width for fission with quantum numbers  $J\pi$  in the case of total  $K$  mixing is

$$\langle \Gamma_f(EJ\pi) \rangle = \frac{D(EJ\pi)}{2\pi} \sum_{\nu} \left( T_D^{\nu}(EJ\pi) + N_{\text{abs}}(EJ\pi) \times \frac{P_F^{\nu}(EJ\pi)}{\sum_{\nu} [P_A^{\nu}(EJ\pi) + P_F^{\nu}(EJ\pi)]} \right) \quad (19)$$

or, if we substitute

$$N_A = \sum_{\nu} P_A^{\nu}(EJ\pi), \quad N_B = \sum_{\nu} P_B^{\nu}(EJ\pi), \quad (20)$$

$$N_D = \sum_{\nu} T_D^{\nu}(EJ\pi),$$

we get

$$\langle \Gamma_f(EJ\pi) \rangle = \frac{D}{2\pi} \left( N_D + N_{\text{abs}} \frac{N_B}{N_A + N_B} \right) \quad (21)$$

which is the expression used in the calculations.

It is now interesting to see what happens when the strength of the imaginary potential is increased to the limit where the directly transmitted flux  $T_D$  is zero. In this case we get  $P_D = 0$  and  $N_{\text{abs}} = N_A$ , and thus, using Eq. (21) we find

$$\langle \Gamma_f(EJ\pi) \rangle = \frac{D}{2\pi} \frac{N_A N_B}{N_A + N_B}. \quad (22)$$

Inserting Eq. (22) into the expression for the fission probability Eq. (3), we obtain

$$P_f = \sum_{I\pi} \left( \alpha(J\pi) \frac{N_A N_B}{N_A N_B + N_{\gamma} (N_A + N_B)} F \right), \quad (23)$$

where

$$N_{\gamma} = 2\pi \Gamma_{\gamma} / D. \quad (24)$$

It is seen that this expression is identical to the limiting strong-coupling expression used to analyze isomer results.<sup>40</sup>

We have thus shown that our model is an intermediate coupling model, which can be applied to situations spanning the entire coupling range from pure fission motion with resonant barrier penetration to the strong coupling extreme where the fission proceeds in two independent steps: penetration of barrier  $A$  followed by penetration of barrier  $B$ .

### 5. Radiation widths

The width for  $\gamma$  emission is calculated assuming that only  $E1$  transitions are important and that they follow the  $E_{\gamma}^3$  rule. Integrating over the possible final states one obtains the expression

$$\Gamma_{\gamma}(EJ\pi) = CA^{2/3} D(EJ\pi) \times \sum_{J_f = |J-1|}^{J+1} \int_0^E \rho(\epsilon, J_f, -\pi) (E - \epsilon)^3 d\epsilon, \quad (25)$$

where  $J_f$  is the final spin. The normalization constant  $C$  is adjusted to approximately reproduce experimentally known  $\gamma$  widths at the neutron binding energy  $B_n$ . The  $\gamma$  width has almost no dependence

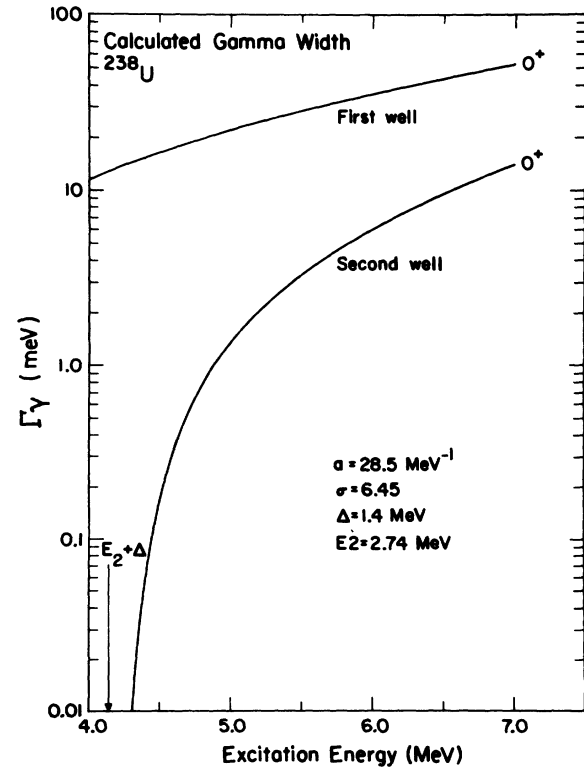


FIG. 9. Calculated  $\gamma$ -decay widths as a function of excitation energy for  $^{238}\text{U}$ .

on the spin and very weak dependence on excitation energy (see Fig. 9).

### 6. Level densities

The level densities in the first well used in the calculations of  $N_\gamma = 2\pi\rho\Gamma_\gamma$  are taken to be of the form

$$\rho(UJ\pi) = \frac{1}{2} \frac{\sqrt{\pi} \exp(2\sqrt{aU})}{12a^{1/4}U^{5/4}} \frac{(2J+1)\exp[-(J+\frac{1}{2})^2/2\sigma^2]}{2\sqrt{2\pi}\sigma^3}, \quad (26)$$

where  $U = E - \Delta_N - \Delta_P$ .

The level-density parameter  $a$ , spin-cutoff factor  $\sigma$ , and pairing corrections  $\Delta_N$  and  $\Delta_P$  are taken from Ref. 41 in the cases where experimental values are known, otherwise from the nearest experimental value. In Table III the values of these parameters are listed for the even-even nuclei together with the resulting level density and  $\gamma$  radiation widths for spin  $0^+$  states at the neutron binding energy.

## 5. COMPARISON BETWEEN THEORY AND EXPERIMENT

### A. Significance of the extracted barrier parameters

Altogether eight parameters (see Fig. 8) enter into the calculations of the fission probabilities, namely  $E_A$ ,  $\hbar\omega_A$ ,  $E_{\min}$ ,  $\hbar\omega_{II}$ ,  $E_B$ ,  $\hbar\omega_B$ ,  $W_0$ , and  $w$ . The predicted  $P_f(E)$  exhibits varying degrees of sensitivity towards these parameters and hence some can be extracted in a fairly unique way while others are left almost undetermined. Experience with the analysis code has given some guidelines,

which are outlined briefly here.

The parameters  $E_{\min}$  and  $\hbar\omega_{II}$  mainly influence the position of a resonance and they enter in a strongly correlated way. Thus it is not possible to obtain independent determinations of  $E_{\min}$  and  $\hbar\omega_{II}$  from the present analysis, even in cases where resonances have been observed. We have chosen  $\hbar\omega_{II}$  values of approximately 1 MeV and treated  $E_{\min}$  as a free parameter which is adjusted to reproduce the experimental resonance positions. However, the resonance positions are also sensitive to the barrier maxima so that these fits do not yield a significant determination of  $E_{\min}$ . In cases where estimates of  $E_{\min}$  are available from fission-isomer data<sup>42, 43</sup> we have restricted our values to agree approximately with the experimental values.

The damping mainly influences the fission probabilities near the resonance energies and again it is not possible to determine both parameters  $W_0$  and  $w$  independently [see Eq. (12)]. Typical values of  $W_0$  used in the calculations are  $0 \leq W_0 \leq 150$  keV while  $w$  values from 0.10 to 0.15 were allowed.

Quantum mechanically a barrier penetration factor does not depend on whether the barrier  $V(\epsilon)$  was approached from the side of large  $\epsilon$  values or from the side of small  $\epsilon$  values. Therefore in the limit of zero damping in the second well, the predicted  $P_f(E)$  are independent of the ordering of the two barriers  $A$  and  $B$ . In practice the damping is finite but the calculated  $P_f(E)$  are still largely independent of the barrier ordering so that in the analysis we have assumed that the outer barrier (larger deformations) is thicker than the inner barrier (i.e., we have assumed that  $\hbar\omega_B < \hbar\omega_A$ ). This assumption is in agreement with the fission isomer lifetimes and excitation functions,<sup>43</sup> with the

TABLE III. Summary of parameters used in the calculation of level densities and  $\gamma$ -decay widths.

| Nucleus           | $B_n$<br>(MeV) | $\Delta_p$<br>(MeV) | $\Delta_n$<br>(MeV) | $a$<br>(MeV <sup>-1</sup> ) | $\sigma$<br>$\hbar$ | $C$<br>(units of $10^{-6}$ MeV <sup>-3</sup> ) | $\rho$ ( $0^+$ )<br>(eV <sup>-1</sup> ) | $D$ ( $0^+$ )<br>(eV) | $\Gamma_\gamma$ ( $0^+$ )<br>(meV) | $2\pi\rho\Gamma_\gamma$ ( $0^+$ )<br>(units of $10^{-3}$ ) |
|-------------------|----------------|---------------------|---------------------|-----------------------------|---------------------|--|---|-----------------------|------------------------------------|--|
| <sup>230</sup> Th | 6.790          | 0.78                | 0.79                | 29.77                       | 6.15                | 0.002  | 0.238                                   | 4.2                   | 39.5                               | 59.1   |
| <sup>232</sup> Th | 6.434          | 0.78                | 0.57                | 29.77                       | 6.15                | 0.002  | 0.172                                   | 5.8                   | 39.1                               | 42.3   |
| <sup>234</sup> Th | 6.179          | 0.78                | 0.49                | 29.77                       | 6.15                | 0.002  | 0.110                                   | 9.1                   | 39.1                               | 27.0   |
| <sup>232</sup> U  | 7.270          | 0.69                | 0.50                | 26.79                       | 6.40                | 0.002  | 0.255                                   | 3.9                   | 68.4                               | 109.5  |
| <sup>234</sup> U  | 6.841          | 0.69                | 0.57                | 26.79                       | 6.40                | 0.002  | 0.111                                   | 9.0                   | 63.6                               | 44.4   |
| <sup>236</sup> U  | 6.390          | 0.69                | 0.49                | 28.51                       | 6.45                | 0.002  | 0.111                                   | 9.0                   | 47.4                               | 33.1   |
| <sup>238</sup> U  | 6.144          | 0.70                | 0.70                | 28.50                       | 6.45                | 0.002  | 0.43                                    | 23.3                  | 37.9                               | 10.2   |
| <sup>240</sup> U  | 5.933          | 0.69                | 0.50                | 31.32                       | 6.20                | 0.002  | 0.141                                   | 7.1                   | 32.2                               | 28.5   |
| <sup>238</sup> Pu | 6.998          | 0.61                | 0.49                | 26.50                       | 6.45                | 0.002  | 0.190                                   | 5.3                   | 68.0                               | 81.2   |
| <sup>240</sup> Pu | 6.534          | 0.61                | 0.43                | 27.41                       | 6.45                | 0.0015   | 0.127                                   | 7.9                   | 42.2                               | 33.7   |
| <sup>242</sup> Pu | 6.300          | 0.61                | 0.50                | 27.93                       | 6.40                | 0.002  | 0.082                                   | 12.2                  | 51.9                               | 26.7   |
| <sup>244</sup> Pu | 6.018          | 0.61                | 0.39                | 27.90                       | 6.35                | 0.002  | 0.063                                   | 15.9                  | 45.1                               | 17.9   |
| <sup>244</sup> Cm | 6.799          | 0.72                | 0.50                | 26.53                       | 6.35                | 0.002  | 0.103                                   | 9.7                   | 65.4                               | 42.3   |
| <sup>246</sup> Cm | 6.210          | 0.72                | 0.39                | 26.53                       | 6.35                | 0.002  | 0.043                                   | 23.3                  | 51.4                               | 13.9   |
| <sup>250</sup> Cm | 5.750          | 0.72                | 0.39                | 28.50                       | 6.35                | 0.002  | 0.032                                   | 30.8                  | 41.0                               | 8.4  |

fission isomer results in the U and Np isotopes,<sup>44</sup> and with most of the theoretical barrier calculations.<sup>6-10</sup> Also this assumption is consistent with our <sup>244, 248</sup>Cm results combined with fission-isomer results for Cm isotopes.<sup>43</sup>

Typical values of  $\hbar\omega_A \sim 0.9$  MeV and  $\hbar\omega_B \sim 0.6$  MeV are most consistent with the wide variety of experimental data available on the fission of doubly even nuclei. Thus the searches on  $\hbar\omega_A$  and  $\hbar\omega_B$  applied in the fitting to the present data have been restricted to values in this vicinity.

With the above restrictions in mind it appears that for cases where resonances are observed, four parameters  $E_A$ ,  $\hbar\omega_A$ ,  $E_B$ , and  $\hbar\omega_B$  can be determined well from analysis of the present data. When no resonances occur, the higher of the two barriers determines  $P_f(E)$  in the threshold region and thus we may derive well-defined values for  $E_B$  and  $\hbar\omega_B$  or  $E_A$  and  $\hbar\omega_A$  depending on which isotopes are analyzed. It is usually possible then to obtain an upper limit for the barrier height that is not directly determined.

The major uncertainties in the values of  $E_A$ ,  $\hbar\omega_A$ ,  $E_B$ , and  $\hbar\omega_B$  stem from ambiguities in the analyses of the fission-probability distributions. Careful analysis has shown that almost equally good agreement with the experimental data can be obtained with barrier heights differing by as much as 200 keV and curvatures differing by as much as 100 keV when compensating changes are made in the other parameter.

Estimates for transition-state energies were first taken from previous fits to angular-correlation results<sup>27, 32</sup> or extrapolated from these values in cases where experimental results are not available. The energies of the lowest transition states were then varied slightly to give best fits to our fission-probability distributions. The actual transition-state energies used in the final fits are listed in Table IV. Comparisons of the calculated fission-fragment angular correlations with the experimentally measured results are shown and discussed in Appendix I.

## B. Details of the Analysis

### 1. Thorium nuclei

The experimental results are shown in comparison with the theoretical calculations in Fig. 10. The <sup>230</sup>Th results are statistically rather poor because of the smallness of the <sup>231</sup>Pa( $t, \alpha$ ) cross section. The calculated curve overestimates the fission probability above  $E = 6.4$  MeV but the analysis still yields the approximate height of the highest peak of the fission barrier (presumably the outer barrier).

For <sup>232</sup>Th the fission probability rises very

abruptly at  $\sim 5$  MeV, a result that is consistent with a high and thick outer barrier dominating the threshold region. A resonance may be present at  $\sim 5.5$  MeV, but since the data are not statistically significant, this possibility has been ignored in the analysis. Above the neutron binding energy  $B_n = 6.43$  MeV the measured fission probability is dropping rapidly below the predicted curve because of the onset of neutron emission.

The <sup>234</sup>Th results show a resonance structure in the fission probability between 5.5 and 5.8 MeV. Above this energy the experimental points rise very steeply until the neutron binding energy is reached at  $B_n = 6.18$  MeV. At higher energies there are strong fluctuations in the fission probability which may partly be due to neutron evaporation and partly to resonance structures. The calculated curve follows the data points quite closely up to the neutron threshold.

### 2. Uranium nuclei

The calculated and experimental fission probabilities are shown in Fig. 10. In <sup>232</sup>U we do not observe any clear resonance structures, but rather a broad shoulder extending from  $E = 5.0$  to 5.5 MeV. In the theoretical calculation the shoulder was assumed to consist of resonances from the two lowest fission channels,  $K = 0^+$  and  $K = 2^+$ . A large maximum value of  $P_f = 0.75$  was observed for the fission probability in <sup>232</sup>U presumably caused by the relatively high-lying position of the neutron threshold at  $B_n = 7.27$  MeV.

The <sup>234</sup>U results, taken from Ref. 31, exhibit a resonance at  $E = 5.0$  MeV which is well reproduced by the calculated curve. Immediately above this energy the theoretical curve deviates from the ex-

TABLE IV. Transition-state energy in keV.

| Nucleus           | $E_{2+}$ | $E_{0-}$ | $E_{1-}$ | $E_{4+}$ | $E_{2-}$ | $E_{3-}$ | $E_{3+}$ |
|-------------------|----------|----------|----------|----------|----------|----------|----------|
| <sup>230</sup> Th | 400      | 200      | 600      |          |          |          |          |
| <sup>232</sup> Th | ...      | 200      | ...      |          |          |          |          |
| <sup>234</sup> Th | 550      | 190      | 400      |          |          |          |          |
| <sup>232</sup> U  | 200      | 700      | 900      | 1000     | 1100     | 1200     | 1300     |
| <sup>234</sup> U  | 300      | 350      | 650      |          |          |          |          |
| <sup>236</sup> U  | 180      | 150      | 450      |          |          |          |          |
| <sup>238</sup> U  | 300      | 400      | 600      |          |          |          |          |
| <sup>240</sup> U  | 300      | 350      | ...      |          |          |          |          |
| <sup>238</sup> Pu | 300      | 400      | 500      | 600      | 700      |          |          |
| <sup>240</sup> Pu | 400      | 600      | 700      | ...      | 1100     |          |          |
| <sup>242</sup> Pu | 250      | 500      | 800      |          |          |          |          |
| <sup>244</sup> Pu | 250      | 400      |          |          |          |          |          |
| <sup>244</sup> Cm | 250      | 450      | 600      |          |          |          |          |
| <sup>248</sup> Cm | 250      | 600      | 800      |          |          |          |          |
| <sup>250</sup> Cm | 250      | ...      | ...      |          |          |          |          |

perimental points while good agreement is reestablished above 5.6 MeV and up to the neutron threshold. A possible explanation for the deviation may be that the assumption of an energy-independent spin-parity distribution is invalid for the  $(d, p)$  reaction (see e.g., Ref. 45).

$^{238}\text{U}$  shows a narrow resonance at 5.0 MeV and a broader structure at 5.15 MeV. In the theoretical analysis it was assumed that the 5.0-MeV resonance has  $K=0^+$  character while the 5.15-MeV structure is composite, having  $K=0^-$  and  $K=2^+$  band contributions. The fit is satisfactory up through the neutron threshold region at 6.39 MeV. The steep slope of the measured  $P_f(E)$  distribution gives rise to relatively small  $\hbar\omega$  values for this nucleus.

Both resonances in  $^{238}\text{U}$  are reproduced under the assumption that they stem from the  $K=0^+$  fission channel. Their energy difference of 0.7 MeV, however, is not a good measure of the frequency in the second well, since this difference depends more sensitively on the parameters  $E_A$ ,  $\hbar\omega_A$ ,  $E_B$ , and  $\hbar\omega_B$  than on  $\hbar\omega_{II}$ . The rapid drop observed in the fission probability above  $B_n=6.14$  MeV is probably caused by the onset of competition from neutron evaporation.

The fission resonance at  $E=5.4$  MeV for  $^{240}\text{U}$  is assumed to be caused by the  $K=0^+$  fission channel. The model is not able to reproduce the very gentle slope observed below the resonance. Otherwise the calculation is in reasonable agreement with the data up to the neutron threshold at  $B_n=5.93$  MeV.

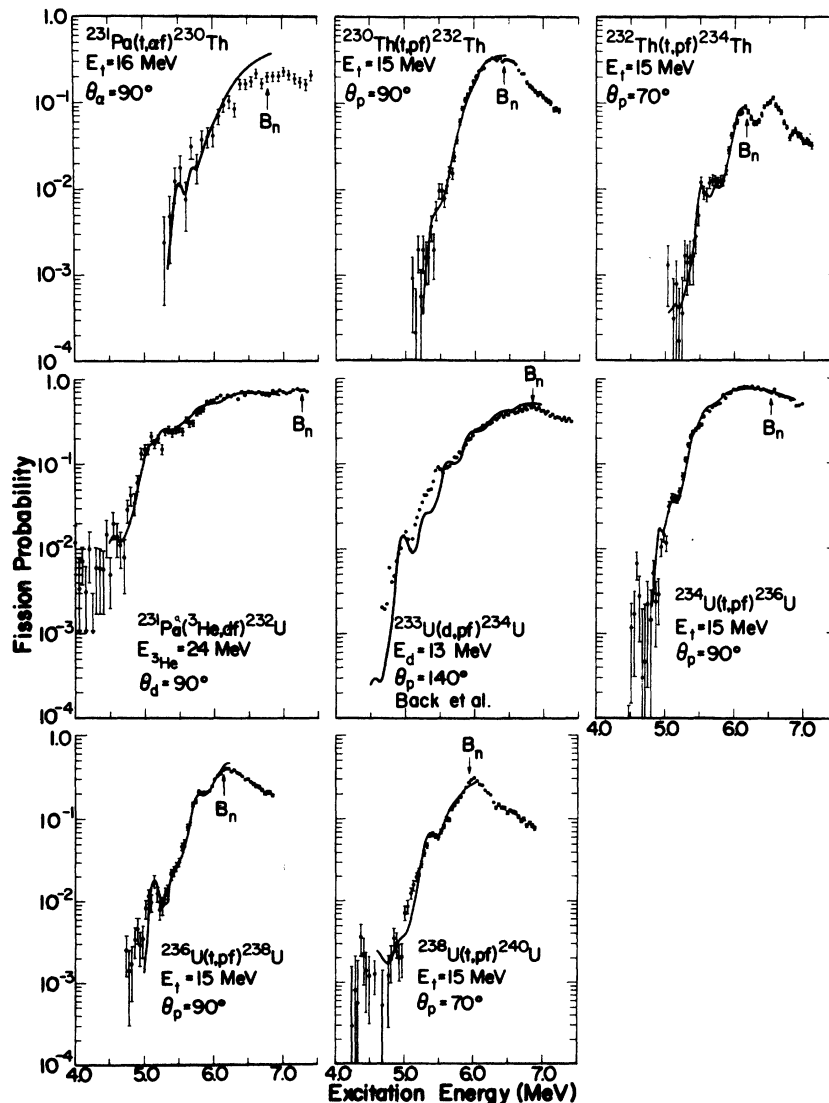


FIG. 10. Fission-probability distributions for thorium and uranium nuclei. Solid curves show fits obtained with the theoretical model described in the text. The  $^{234}\text{U}$  data are taken from Ref. 31.

### 3. Plutonium nuclei

The fits to the Pu results are shown in Fig. 11. The  $^{238}\text{Pu}$  results show a very gentle slope in the threshold region with a weak indication of a resonance at  $E = 5.1$  MeV. The high value of  $B_n = 7.00$  MeV ensures a large maximum value of the fission probability  $P_{f,\text{max}} = 0.8$ . The calculated curve is in good agreement with the experimental results in the entire region below  $B_n$ .

For systematic reasons we include the analysis of previous  $^{240}\text{Pu}$  results.<sup>27</sup> The resonance at  $E = 5.0$  MeV is reproduced and good agreement be-

tween measurement and theory is obtained.

The resonance observed in  $^{242}\text{Pu}$  at  $E = 4.65$  MeV is reproduced assuming  $K = 0^+$  character. The shoulder at  $E = 4.9$  MeV is interpreted as being caused by the  $K = 2^+$  channel. Above  $E = 5.3$  MeV there are some deviations between theory and data. These discrepancies could in part be due to a poor determination of the singles cross section in this energy region (see Fig. 5).

In  $^{244}\text{Pu}$  the calculated curve follows the general trend of the experimental points, but fails to reproduce some of the fine details. Possible reasons for this is discussed in Sec. 4 A 2. Because

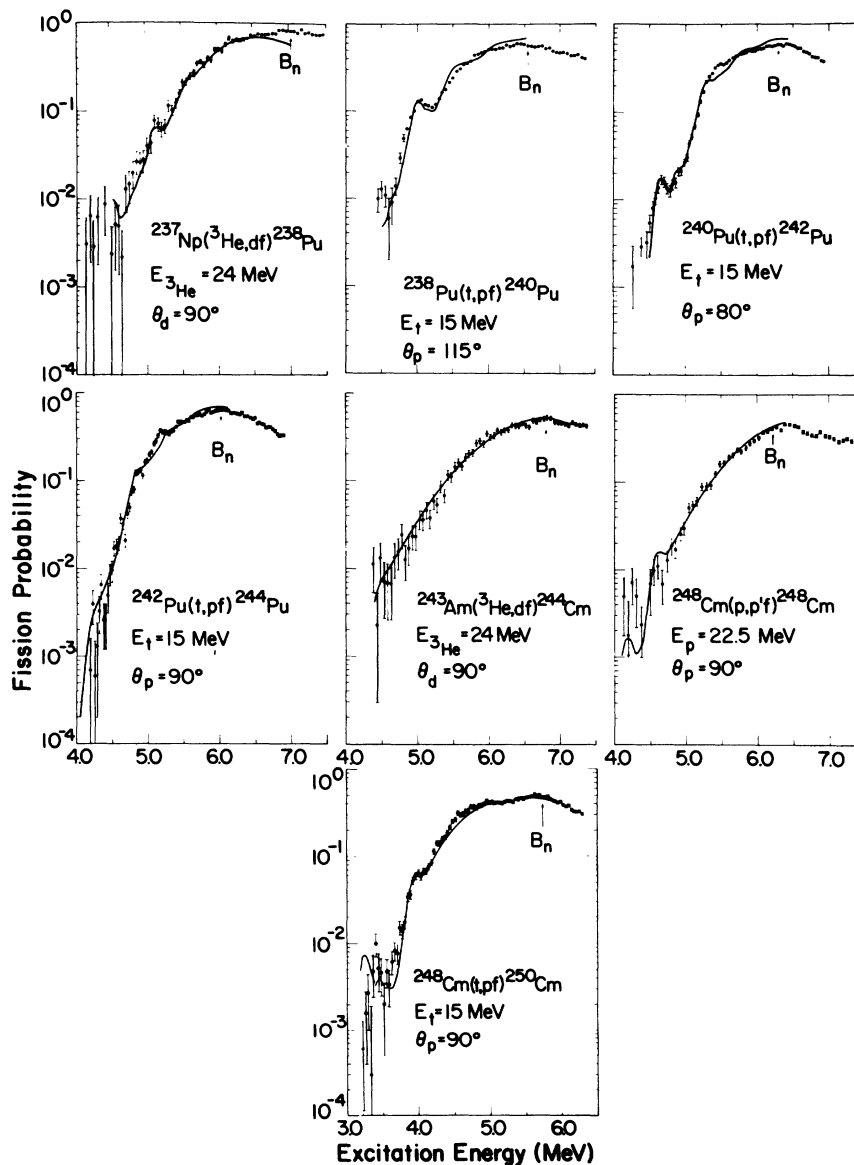


FIG. 11. Fission-probability distributions for plutonium and curium nuclei. Solid curves show fits obtained with the theoretical model described in the text. The  $^{240}\text{Pu}$  data are taken from Ref. 27.

the over-all characteristics of the measurement are reproduced, we believe that the parameters extracted for the fission barrier are reasonable.

#### 4. Curium nuclei

The results from fits to Cm nuclei are shown in Fig. 11. Analysis of the excitation function for populating the fission isomers in  $^{241}, ^{243}, ^{245}\text{Cm}$  (Ref. 43) yields values of the height of the second barrier of  $E_B = 4.2$ ,  $E_B = 4.0$ , and  $E_B = 4.4$  MeV, respectively. Using a similar value ( $E_B = 4.5$  MeV) in the case of  $^{244}\text{Cm}$  and adjusting  $E_A$  and  $\hbar\omega_A$  to give the observed threshold behavior we find that no resonance structure is predicted in agreement with the experimental results. The data require a first barrier approximately 2 MeV higher than the second and this makes the penetrability in the region of interest look as if calculated for a single barrier.

For  $^{248}\text{Cm}$  the first barrier is also approximately 1.6 MeV higher than the assumed value  $E_B = 4.5$  MeV extrapolated from Ref. 43. This leads to a smooth curve for the fission probability which agrees well with the experiment. The calculation predicts a shoulder at  $E = 4.6$  MeV which is not in disagreement with the data.

The drastic change in the fission threshold (see Fig. 12) observed in going from  $^{248}\text{Cm}$  to  $^{250}\text{Cm}$  is caused mainly by a 1.0-MeV drop in the height of the first barrier (see also Ref. 19). Since the difference between the two barriers is thereby decreased, a (resonant) plateau in the fission probability is generated at  $E = 4.0$  MeV which is also apparent in the data. The  $^{250}\text{Cm}$  results also exhibit

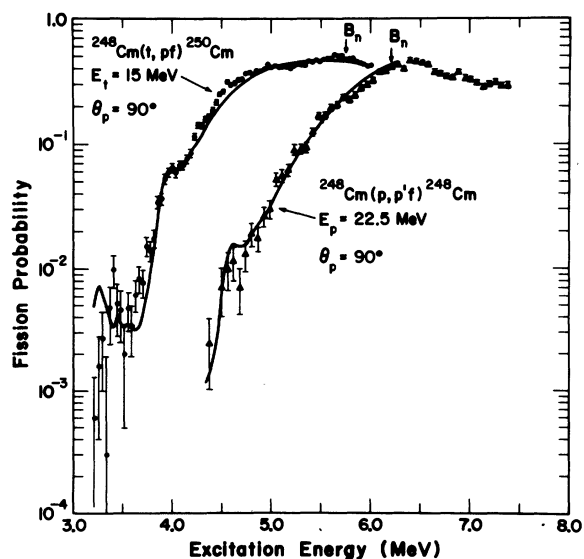


FIG. 12. Comparison of fission-probability distributions for  $^{250}\text{Cm}$  and  $^{248}\text{Cm}$ .

a narrow resonance at  $E = 3.4$  MeV. Unfortunately this energy coincides with a strong contaminant peak in the singles spectrum (see Fig. 5), which casts some doubt on the existence of this resonance even though it persists after the proper correction for accidental coincidences. As in the result for  $^{240}\text{U}$  we predict a steeper slope just below the resonance at  $E = 4.0$  MeV than is observed experimentally.

#### 6. DISCUSSION

The barrier parameters obtained from the analysis of experimental results can be compared to the theoretical calculations of static potential-energy surfaces performed by many groups. However, in doing this it should be remembered that the model used in the analysis of the data contains several simplifications that could affect the extracted values of the barrier parameters in a systematic way (see Sec. 4 A). The major oversimplifications are the assumptions of a single barrier shape (see Sec. 4 A2) and the assumption of strong coupling between levels in the first and second potential well (see Appendix II). In both cases tests of the effects of trying to relax these assumptions have indicated only small changes in  $E_A$  and  $E_B$ , but indicated that the  $\hbar\omega$  values determined could be

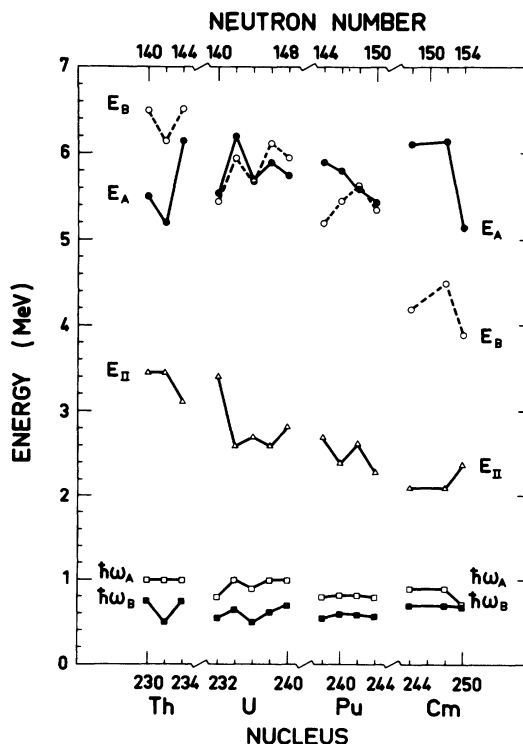


FIG. 13. Fission-barrier parameters determined from the analysis of the experimental results.

systematically underestimated by ~10%.

A qualitative estimate of the possible model dependence can be obtained by comparing our extracted barrier parameters with those obtained previously. The results of such a comparison are shown in Table V for the nuclei on which information was previously available. The current barriers are compared to previous estimates from two different sources: First, values of  $E_B$  obtained from the analysis of fission-isomer excitation functions. In the case of  $^{238}\text{Pu}$  and  $^{240}\text{Pu}$  it is seen that barrier estimates from the two independent types of experiment agree quite well. The other comparisons are to previous direct-reaction induced-fission data which were analyzed with much more simplified statistical models. An estimate of the over-all agreement between the barrier parameters from various analyses is obtained from the mean value of the standard deviation  $\bar{\sigma}$  of the parameters in Table V. It is seen that the values of  $\bar{\sigma}$  lie well within the uncertainties estimated for the presently quoted parameters.

In this model we essentially assume that fission near threshold follows a single one-dimensional path and in comparing our barrier parameters

with theoretically calculated *static* barriers we further assume that this path goes over the two static saddle points. Recent trajectory calculations<sup>46</sup> have suggested that the dynamic barriers associated with spontaneous fission may be different from the static barriers obtained from potential-energy calculations. However, this effect should be of less importance for fission near threshold.

The barrier parameters used to reproduce the experimentally measured fission-probability curves are shown in Fig. 13. We emphasize that not all of these parameters should be regarded as measured in the present experiment as discussed in Sec. 5 A. We merely show them to illustrate that the measured fission-probability curves are consistent with smooth systematic trends of the parameters. The quantities which are determined with significant accuracy from the analysis of the experimental data are given in Table VI.

The most striking feature about the height of the first barrier is the constancy throughout the whole region from Th to Cm. There are only relatively small deviations away from an average value of  $E_A \approx 5.8 \text{ MeV}$ , but some of them are significant.

TABLE V. Comparison of fission-barrier parameters extracted from different experiments. Energies are in MeV.

| Nucleus                                   | $E_A$ | $E_B$ | $\hbar\omega_A$ | $\hbar\omega_B$ | Reaction                      | Reference |
|---|-------|-------|-----------------|-----------------|-------------------------------|-----------|
| $^{232}\text{Th}$                         |       | 6.15  |                 | 0.50            | ( <i>t,p</i> )                | a         |
| $^{232}\text{Th}$                         |       | 5.75  |                 | 0.43            | ( <i>t,p</i> )                | b         |
| $^{234}\text{Th}$                         |       | 6.50  |                 | 0.75            | ( <i>t,p</i> )                | a         |
| $^{234}\text{Th}$                         |       | 6.05  |                 | 0.43            | ( <i>t,p</i> )                | b         |
| $^{234}\text{U}$                          | 6.20  | 5.95  | 1.00            | 0.65            | ( <i>d,p</i> )                | a         |
| $^{234}\text{U}$                          | 6.20  | 5.95  | 1.00            | 0.70            | ( <i>d,p</i> )                | c         |
| $^{236}\text{U}$                          | 5.70  | 5.70  | 0.90            | 0.50            | ( <i>t,p</i> )                | a         |
| $^{236}\text{U}$                          | 6.10  | 5.80  | 1.00            | 0.70            | ( <i>d,p</i> )                | c         |
| $^{238}\text{U}$                          | 5.90  | 6.10  | 1.00            | 0.62            | ( <i>t,p</i> )                | a         |
| $^{238}\text{U}$                          | 5.77  | 5.65  | 0.80            | 0.47            | ( <i>t,p</i> )                | b         |
| $^{240}\text{U}$                          | 5.75  | 5.95  | 1.00            | 0.70            | ( <i>t,p</i> )                | a         |
| $^{240}\text{U}$                          | 5.80  | 5.60  | 0.95            | 0.47            | ( <i>t,p</i> )                | b         |
| $^{238}\text{Pu}$                         |       | 5.20  |                 | 0.55            | ( <i>t,p</i> )                | a         |
| $^{238}\text{Pu}$                         |       | 5.35  |                 | 0.73            | Isomer                        | d         |
| $^{240}\text{Pu}$                         | 5.80  | 5.45  | 0.82            | 0.60            | ( <i>t,p</i> )                | a         |
| $^{240}\text{Pu}$                         | 5.95  | 5.25  | 1.30            | 0.48            | ( <i>d,p</i> )( <i>p,p'</i> ) | e         |
| $^{240}\text{Pu}$                         |       | 5.55  | 1.00            | 0.70            | ( <i>d,p</i> )                | c         |
| $^{240}\text{Pu}$                         |       | 5.35  |                 | 0.68            | Isomer                        | d         |
| $^{242}\text{Pu}$                         | 5.60  | 5.65  | 0.82            | 0.59            | ( <i>t,p</i> )                | a         |
| $^{242}\text{Pu}$                         | 5.60  | 5.05  | 1.25            | 0.42            | ( <i>t,p</i> )                | b         |
| $^{242}\text{Pu}$                         | 6.10  | 5.50  | 1.00            | 0.70            | ( <i>d,p</i> )                | c         |
| $^{244}\text{Pu}$                         | 5.45  | 5.35  | 0.80            | 0.57            | ( <i>t,p</i> )                | a         |
| $^{244}\text{Pu}$                         | 5.55  | 4.90  | 1.25            | 0.40            | ( <i>t,p</i> )                | b         |
| Mean value<br>of standard deviation value | 0.105 | 0.155 | 0.085           | 0.088           |                               |           |

<sup>a</sup> Present work.

<sup>b</sup> Cramer and Britt, Ref. 27.

<sup>c</sup> Back *et al.*, Ref. 31.

<sup>d</sup> Britt *et al.*, Ref. 43.

<sup>e</sup> Britt, Burnett, and Cramer, Ref. 32.

Most prominent is the drop of approximately 1.0 MeV occurring between  $^{248}\text{Cm}$  and  $^{250}\text{Cm}$ . As discussed previously<sup>19</sup> approximately 600 keV of this effect is due to the  $N=152$  subshell at the ground-state deformation and the remaining  $\sim 400$  keV is probably due to an antishell at the first maximum occurring at neutron number  $N=150-152$ . In the U isotopes there appear to be high barriers (both first and second) for  $N=142, 146$  and low barriers for  $N=140, 144, 148$ . The barriers for  $^{234}\text{U}$  may be more uncertain due to the problem in defining the spin-parity distribution for the  $(d, p)$  reaction.

In contrast to the constancy for the first maximum, the second maximum shows a regular decreasing pattern in going from  $^{230}\text{Th}$  to  $^{250}\text{Cm}$ . Thus the relative height of the two maxima is shifted in the sense that the threshold behavior in the Th isotopes is dominated by the second barrier, in the U and Pu isotopes both barriers play a strong role, and in Cm the first barrier dominates fission near threshold.

The fission-isomer energy  $E_{\text{II}}$  is not well determined, as pointed out in Sec. 5 A, but as seen in Fig. 13 the values used follow a smooth trend in going from  $^{230}\text{Th}$  to  $^{250}\text{Cm}$ . The barrier curvatures  $\hbar\omega_A$  and  $\hbar\omega_B$  show only small deviations from mean values of  $\hbar\omega_A \approx 0.90$  MeV and  $\hbar\omega_B \approx 0.62$  MeV over the region investigated.

When trying to understand the deviations from smooth trends of experimentally measured fission barriers it is important to realize that these are measured relative to the energy of the deformed ground state. Consequently, fluctuations in the ground-state shell correction and the saddle-point

shell correction both show up in the experimental fission barriers. To independently study the shell effects at the fission barriers one should measure the barrier heights relative to the prediction of the liquid-drop model which contains no shell effects.

Barrier parameters  $E_A - \bar{E}_0$  and  $E_B - \bar{E}_0$ , where  $\bar{E}_0$  is the energy of the spherical liquid-drop nucleus,<sup>47</sup> are plotted in Fig. 14 versus the fissility parameter  $X = (Z^2/A)/(Z^2/A)_{\text{crit}}$ . It is seen that the second barrier  $E_B - \bar{E}_0$  follows rather closely the liquid-drop barrier of Ref. 48. This means that the change in liquid-drop energy  $\Delta E_{\text{LD}} \equiv E_{\text{LD}}^B - E_{\text{LDS}}$  going from liquid-drop saddle ( $E_{\text{LDS}}$ ) to the actual second saddle ( $E_{\text{LD}}^B$ ) is balanced by the shell-correction energy at this point ( $E_{\text{shell}}^B$ ):

$$E_{\text{shell}}^B \approx E_{\text{LD}}^B - E_{\text{LDS}}. \quad (27)$$

A similar systematics is found for the experimental fission barriers in lighter nuclei.<sup>49</sup>

In contrast to this the first barrier  $E_A - \bar{E}_0$  does not follow the trend of the liquid-drop barrier so closely but changes only about 1 MeV from Th to Cm. In the Cm isotopes it is approximately 1.5 MeV higher than the liquid-drop barrier, which in-

TABLE VI. Fission-barrier parameters from the analysis of experimental data.  $E_A$  and  $E_B$  are measured relative to the energy of the ground state. Energies are in MeV.

| Nucleus           | $E_A$           | $E_B$           | $\hbar\omega_A$ | $\hbar\omega_B$ |
|-------------------|-----------------|-----------------|-----------------|-----------------|
| $^{230}\text{Th}$ |                 | $6.5 \pm 0.3$   |                 |                 |
| $^{232}\text{Th}$ | $<5.50$         | $6.15 \pm 0.20$ |                 | $0.50 \pm 0.10$ |
| $^{234}\text{Th}$ | $6.15 \pm 0.20$ | $6.52 \pm 0.20$ | $1.00 \pm 0.10$ | $0.75 \pm 0.10$ |
| $^{232}\text{U}$  | $5.54 \pm 0.20$ | $5.45 \pm 0.20$ | $0.80 \pm 0.10$ | $0.55 \pm 0.10$ |
| $^{234}\text{U}$  | $6.20 \pm 0.25$ | $5.95 \pm 0.25$ | $1.00 \pm 0.10$ | $0.65 \pm 0.10$ |
| $^{236}\text{U}$  | $5.70 \pm 0.20$ | $5.68 \pm 0.20$ | $0.90 \pm 0.10$ | $0.50 \pm 0.10$ |
| $^{238}\text{U}$  | $5.90 \pm 0.20$ | $6.12 \pm 0.20$ | $1.00 \pm 0.10$ | $0.62 \pm 0.10$ |
| $^{240}\text{U}$  | $5.75 \pm 0.20$ | $5.95 \pm 0.20$ | $1.00 \pm 0.10$ | $0.70 \pm 0.10$ |
| $^{238}\text{Pu}$ | $5.90 \pm 0.20$ | $5.20 \pm 0.30$ | $0.80 \pm 0.10$ | $0.55 \pm 0.10$ |
| $^{240}\text{Pu}$ | $5.80 \pm 0.20$ | $5.45 \pm 0.20$ | $0.82 \pm 0.10$ | $0.60 \pm 0.10$ |
| $^{242}\text{Pu}$ | $5.60 \pm 0.20$ | $5.63 \pm 0.20$ | $0.82 \pm 0.10$ | $0.59 \pm 0.10$ |
| $^{244}\text{Pu}$ | $<5.6$          | $5.35 \pm 0.20$ |                 | $0.57 \pm 0.10$ |
| $^{244}\text{Cm}$ | $6.12 \pm 0.20$ | $<4.9$          | $0.90 \pm 0.10$ |                 |
| $^{248}\text{Cm}$ | $6.15 \pm 0.20$ | $<4.6$          | $0.90 \pm 0.10$ |                 |
| $^{250}\text{Cm}$ | $5.15 \pm 0.20$ | $3.90 \pm 0.30$ | $0.72 \pm 0.10$ | $0.69 \pm 0.10$ |

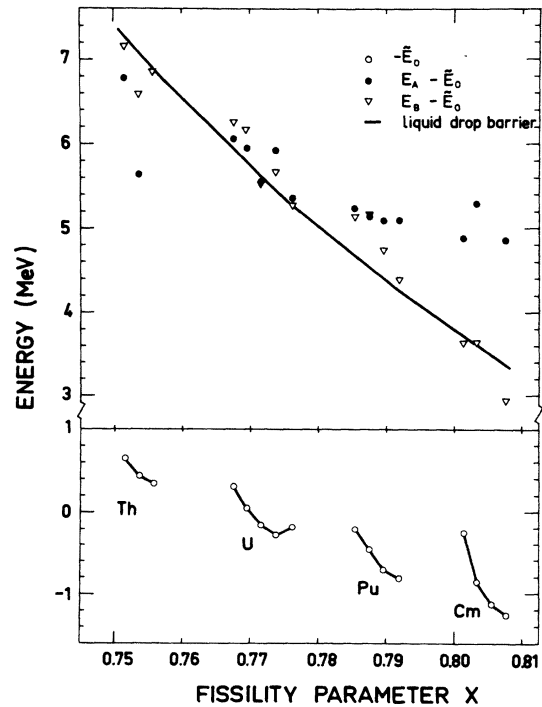


FIG. 14. Heights for the two peaks of the fission barrier measured relative to the spherical liquid-drop energy  $\bar{E}_0$ . The solid curve shows fission barriers predicted by the liquid-drop model (Ref. 48). Also shown are ground-state energies relative to  $\bar{E}_0$ .

dicates that the shell-correction energy is at least 1.5–2.0 MeV at the first barrier in this case.

In addition it is possible to compare the experimentally measured barriers of Th, U, Pu, and Cm nuclei with recent theoretical predictions of Pauli and Ledergerber<sup>9</sup> and Möller and Nix.<sup>50</sup> In Fig. 15 the barriers for even-even nuclei obtained in this experiment, barriers for odd- $A$  nuclei reported in a subsequent publication,<sup>17</sup> and  $E_B$  values from the analysis of fission-isomer results<sup>43</sup> are compared to various theoretical predictions. These theoretical calculations are of three general types: (1) Pauli and Ledergerber use a Woods-Saxon potential and adjust the constants of the surface-asymmetry term of the liquid-drop model to reproduce experimental fission barriers; (2) Möller and Nix use a harmonic-oscillator potential and the recent droplet model of Myers and Swiatecki<sup>51</sup>; and (3) Möller and Nix also present calculations using a folded Yukawa potential and the droplet model. The calculations (1) and (2) have been corrected for effects of axially asymmetric deformations [in the case of (2) the corrections are made using recent results of Larsson and Leander<sup>52</sup>] and for the set (3) this effect has not been considered. Therefore, the results from (3) for  $E_A$  in curium and plutonium nuclei would be further

lowered by this effect. A detailed description of the calculations and comparisons with a wider range of experimental results have been given recently by Möller and Nix.<sup>50</sup> Figure 15 shows that for plutonium and curium nuclei the calculations agree with each other and with the experimental results to an accuracy of  $\sim 1$  MeV. For uranium nuclei the calculated  $E_A$  values are  $\sim 1$ –2 MeV too low and for thorium nuclei the calculations underestimate  $E_A$  by  $\sim 2$ –3 MeV. This “thorium anomaly” was recently discussed by Möller and Nix<sup>50</sup> and they suggest that the Th results may be dominated by a third minimum located near the second asymmetric saddle point.

In summary, we have presented in this paper a set of experimental fission-probability distributions from a variety of doubly even isotopes of Th, U, Pu, and Cm. These and a few previously available results are analyzed with a statistical model in order to obtain a consistent set of experimental values for the fission-barrier parameters  $E_A$ ,  $E_B$ ,  $\hbar\omega_A$ , and  $\hbar\omega_B$ . Comparisons with recent theoretical estimates of  $E_A$  and  $E_B$  indicate very good agreement for plutonium and curium isotopes, but systematic deviations of  $\sim 2$  MeV in the thorium region with uranium cases being intermediate.

## 7. ACKNOWLEDGMENTS

We are grateful to J. Lerner and A. Friedman at Argonne National Laboratory for producing the <sup>240</sup>Cm target. It is a pleasure to acknowledge useful discussions with S. Bjørnholm, A. Bohr, B. M. B. Mottelson, and J. R. Nix. We would like to thank J. E. Lynn for pointing out the effects of various coupling limits on our calculations. We are grateful to B. H. Erkkila for help in initially setting up these experiments. One of us (B.B.B.) is indebted to Statens naturvidenskabelige Forskningsråd, Denmark, for financial support and one of us (H.C.B.) gratefully acknowledges travel support from The Japan World Exhibition Commemorative Association, Tokyo, Japan, during the preparation of this manuscript.

## APPENDIX I. FISSION-FRAGMENT ANGULAR CORRELATIONS

In addition to the fission-probability distributions, which are presented and analyzed in this paper, there also exist empirical information on the angular correlations of the fission fragments for many ( $t, pf$ ) cases.<sup>12, 27</sup> The theoretical model discussed in Sec. 4 also makes definite predictions for the energy dependence of the angular-correlation coefficients and these predictions can be compared with experimental results. In order to make the calculations tractable and reduce the number

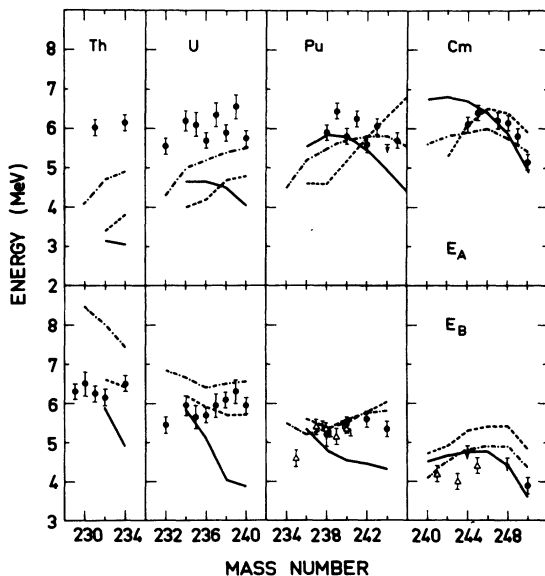


FIG. 15. Fission barriers  $E_A$  and  $E_B$  determined from the analysis of the experimental results (circles) and from previous fits to fission-isomer data (triangles) (see Ref. 43). Solid curve, dash-dot curve, and dash curve show the theoretical predictions by Möller and Nix with a Yukawa potential (Ref. 50); Möller and Nix with a harmonic-oscillator potential (Ref. 50); and Pauli and Ledergerber with a Woods-Saxon potential (Ref. 9), respectively.

of free parameters, several simplifying assumptions were made in developing our model. A few of these simplifications are of minor importance in the fission probability calculations but could have a major influence on the reliability of angular-correlation calculations.

In this Appendix we compare the predictions from our model for the angular-correlation coefficients with previous experimental data for typical cases. The predictions are based on the fits to the fission-probability distributions and no attempts are made to try to simultaneously reproduce the angular correlations. Instead these comparisons are used only to (1) illustrate what general improvements are probably needed in the model in order to attempt serious calculations of the angular correlations and (2) give some indications as to what additional information might be forthcoming from a detailed analysis of both fission-probability and angular-correlation results.

The limiting assumptions in our model which probably have the most serious effect on the reliability of the angular correlation calculations are (1) the assumption that all transition states have the same shape fission barrier; (2) the assumption of strong coupling between the two wells when calculating the damping in the second well (see Appendix II for further discussion of this effect); and (3) the assumption of complete  $K$  mixing in the second well. As discussed below violations of this first assumption may have profound qualitative effects on the angular correlations. Violations of the second and third assumptions will have more subtle effects which we have not investigated in detail but clearly these effects must be looked at more carefully before a serious attempt is made to analyze the angular-correlation data.

In calculating the angular correlations with our model we have followed exactly the formalism given previously.<sup>12, 27</sup> The correlations are expressed as coefficients  $g_{2\lambda}$  in a Legendre polynomial expansion of the fission-fragment angular correlation of the form

$$W(\theta) = A_0 \left[ 1 + \sum_{\lambda} g_{2\lambda} P_{2\lambda}(\cos\theta) \right].$$

For  $^{238}\text{U}$  and  $^{242}\text{Pu}$  the predictions for the coefficients  $g_2$ ,  $g_4$ ,  $g_6$ , and  $g_8$  are shown in Fig. 16 as a function of excitation energy along with experimental data from Cramer.<sup>27</sup> These predictions were obtained with the parameters listed in Tables IV and VI which resulted from the analysis of the fission-probability distributions for energies below the neutron threshold.

The  $^{238}\text{U}$  experimental results seem to agree reasonably well with the model predictions except that the sharp decrease observed in  $g_2$  and  $g_4$  at

6.2 MeV is predicted about 0.2 MeV higher and  $g_6$  is underestimated in the sub-barrier resonance region. The decrease in  $g_2$  and  $g_4$  occurs with the onset of fission through a  $K = 2^+$  transition-state band and the large experimental values of  $g_6$  at 5.5 MeV could be reproduced by a stronger  $K = 0^-$  resonance. Thus, both of these discrepancies may result from the requirement that the fission barrier has the same shape for  $K = 0^+$ ,  $0^-$ , and  $2^+$  bands.

For  $^{242}\text{Pu}$  there is a much larger discrepancy for  $g_4$  and  $g_8$  between the model predictions and the experimental results. Basically the experimental angular distributions show contributions from  $K = 2^+$  transition states in the sub-barrier excitation-energy region, while our model predicts that they will not become important until the excitation energy is increased considerably more. The present model is not capable of reproducing this aspect of the experimental angular-correlation results while still preserving the approximate fit to the fission-probability distributions.

Comparisons between predictions and experimental results for other U and Pu isotopes show similar effects. Thus, the angular-correlation results are reasonably well reproduced by the model for U isotopes but not for Pu isotopes. Similarly, as was discussed in Sec. 5, the fits to the fission probabilities are generally somewhat better for

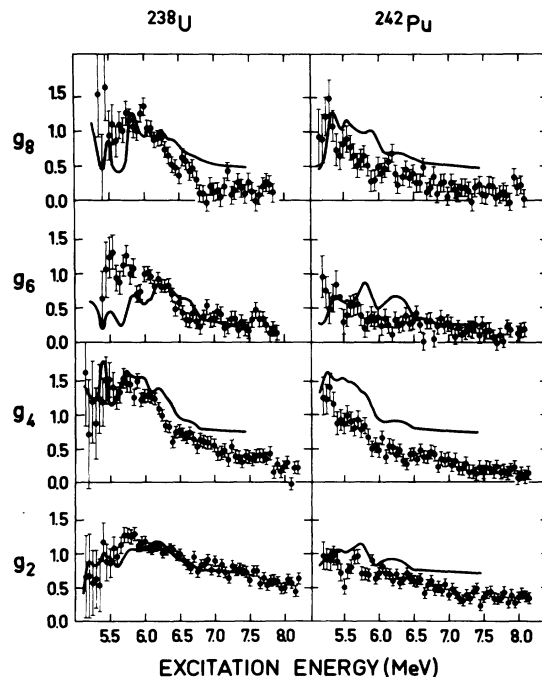


FIG. 16. Predicted angular-correlation coefficients (solid curves) and experimental results from Ref. 27 (points) for  $^{238}\text{U}(t, pf)$  and  $^{240}\text{Pu}(t, pf)$  reactions.

the U isotopes than for the Pu isotopes. These effects could be the result of the expected transition<sup>37, 38</sup> from  $\gamma$ -stable to  $\gamma$ -unstable shapes at the first barrier. Recent calculations<sup>37, 38</sup> indicate that the <sup>238</sup>U nucleus may be stable with respect to a  $\gamma$ -type deformation and <sup>242</sup>Pu unstable. This  $\gamma$  instability would tend to lower the excitation of the  $K = 2^+$  vibration at the first saddle and thus change the shape of the fission barrier for fission through  $K = 2^+$  transition states. A very limited study of this effect for Pu isotopes indicated that it might be possible to reproduce both the fission-probability and angular-correlation results if it is assumed that there is a  $K = 2^+$  barrier different from the  $K = 0^+$  barrier with the relative energy  $E(K = 2^+) - E(K = 0^+)$  being  $\sim 0$  and  $\sim 0.5 - 1.0$  MeV at the first and second saddle points, respectively.

Thus, it seems likely that attempts to simultaneously fit fission-probability and angular-correlation data could yield more detailed information on fission-barrier properties. In addition, the results shown in Fig. 16 suggest that pronounced resonance structure may appear in the correlation coefficients if measurements are performed with better energy resolution and statistical accuracy.

## APPENDIX II. EFFECTS OF COUPLING BETWEEN LEVELS IN THE FIRST AND SECOND WELLS

### A. Coupling problem

It has been pointed out by Lynn<sup>53</sup> that transitions from states in the first well (class I states) to states in the second well (class II states) may be strongly reduced in the limit where the average width of class II levels is much smaller than the average spacing of these levels.

This effect comes about because in this limit it will often happen that there is no class II state which corresponds in energy, spin, and parity to the class I state formed by the initial direct reaction. Thus, the class I state may only be able to decay into the second well because the finite width of the class II states will present a small transition amplitude at the excitation energy  $E$  of the class I state.

One is therefore forced to take into account the Lorentzian tails present at the energy  $E$  from all class II states of the correct spin and parity to match the decaying class I state. (It is, of course, essential that the decay from the first well into the second well does not change the energy of the state.)

In order to estimate the influence of this "mismatch" effect on the fission-probability distributions, we have developed a schematic model that is presented in the next subsection. This model

is valid in the limit where statistical fluctuations in the class II level spacing  $D_{II}$  and the fission width  $\Gamma_f$  are neglected and where the excitation energy in the second well ( $E - E_{II}$ ) is large compared to  $D_{II}$ .

After the derivation of the general expression for  $P_f(E)$  in the next subsection, various limiting situations are discussed, and finally in Subsec. C some test calculations of  $P_f(E)$  are shown and it is concluded that the mismatch effect mainly affects the extracted  $\hbar\omega$  values and the damping in well II, while the barrier heights are insensitive to this refinement.

### B. General expression for $P_f$

According to Eqs. (9) and (10) in Sec. 4 B 3 the fission width can be written as

$$\Gamma_f = \frac{D_I}{2\pi} N_f, \quad (A1)$$

where  $N_f$  is the number of open fission channels

$$N_f = \sum_{\nu} T_f^{\nu}. \quad (A2)$$

Assuming complete  $K$  mixing in the second well we have from Eq. (21)

$$N_f = N_D + N_{\text{abs}} \frac{N_B}{N_A + N_B}. \quad (A3)$$

A possible way to take the effect of coupling between the states in the two wells into account is to multiply  $N_{\text{abs}}$  of Eq. (A3) with a weight function  $f(E, W, D_{II})$  depending on the excitation energy  $E$ , the natural width  $W$ , and the average energy spacing  $D_{II}$  of the class II states. The weight function  $f(E, W, D_{II})$  must be normalized so that

$$\langle f(E, W, D_{II}) \rangle = 1, \quad (A4)$$

where the average is taken over an energy interval containing many class II states.

The weight function  $f(E, W, D_{II})$  is defined by adding the Lorentzian tails from all the class II states:

$$f(x, W, D_{II}) = \frac{D_{II}W}{\pi} \sum_{n=-\infty}^{\infty} \frac{1}{(nD_{II} + x)^2 + W^2}, \quad (A5)$$

where  $x = E - E_0$  and  $E_0$  is the centroid excitation energy of a class II state. The other class II levels are assumed to lie equidistant above and below this reference level with an energy spacing  $D_{II}$ . The width of the class II levels is  $W$  and will be taken equal to the sum of the decay widths from well II at energy  $E$  through the first and second peaks of the fission barrier. Each term in Eq. (A5) represents the intrinsic probabilities that a particular class II state ( $E_x = E_0 + nD_{II}$ ) is populated in the decay from the initial class I level. It is assumed

that the various class II states do not contribute coherently. The summation in Eq. (A5) from  $n = -\infty$  to  $n = +\infty$  will lead to a convenient mathematical expression for  $f(x, W, D_{II})$  but it incorporates the unphysical assumption that the well II is in-

finitely deep and that  $W$  and  $D_{II}$  are constant. However, test calculations have shown that this series converges rapidly and this assumption does not appreciably affect the result.

Observing that the right-hand side of Eq. (A5) can

be split in three parts we get

$$\begin{aligned} f(x, W, D_{II}) \frac{\pi}{WD_{II}} &= \frac{1}{x^2 + W^2} + \sum_{n=1}^{\infty} \left[ \frac{1}{(nD_{II} + x)^2 + W^2} + \frac{1}{(nD_{II} - x)^2 + W^2} \right] \\ &= \frac{1}{x^2 + W^2} + \frac{1}{2iWD_{II}} \sum_{n=1}^{\infty} \left[ \frac{1}{n + x/D_{II} - i(W/D_{II})} - \frac{1}{n + x/D_{II} + i(W/D_{II})} + \frac{1}{n - x/D_{II} - i(W/D_{II})} \right. \\ &\quad \left. - \frac{1}{n - x/D_{II} + i(W/D_{II})} \right]. \end{aligned} \quad (A6)$$

Each of the four sums in the above expression can be replaced by a Digamma function  $\psi(Z)$  of the form

$$\psi(1+b) = - \sum_{n=1}^{\infty} \frac{1}{n+b}. \quad (A7)$$

Using the relation  $\psi(\bar{Z}) = \bar{\psi}(Z)$  (complex conjugate) we find

$$f(x, W, D_{II}) \frac{\pi}{WD_{II}} = \frac{1}{x^2 + W^2} + \frac{1}{2iWD_{II}} \left[ 2 \operatorname{Im} \psi \left( 1 + \frac{x}{D_{II}} + i \frac{W}{D_{II}} \right) - 2 \operatorname{Im} \psi \left( 1 - \frac{x}{D_{II}} - i \frac{W}{D_{II}} \right) \right]. \quad (A8)$$

The Digamma function  $\psi(Z)$  has the following properties

$$\psi(1-z) = \psi(z) + \pi \cot(\pi z) \quad \text{and} \quad \psi(1+z) = \psi(z) + 1/z. \quad (A9)$$

Using these properties we find that Eq. (A8) reduces to

$$\begin{aligned} f(x, W, D_{II}) &= \frac{WD_{II}}{\pi(x^2 + W^2)} + \frac{1}{i\pi} \operatorname{Im} \left( \frac{D_{II}}{x + iW} - \pi \frac{\sin(2\pi x/D_{II}) - i \sinh(2\pi W/D_{II})}{\cosh(2\pi W/D_{II}) - \cos(2\pi x/D_{II})} \right) \\ &= \frac{\sinh(2\pi W/D_{II})}{\cosh(2\pi W/D_{II}) - \cos(2\pi x/D_{II})}. \end{aligned} \quad (A10)$$

It is seen that this form of  $f(x, W, D_{II})$  has the correct normalization of Eq. (A4) because

$$\frac{1}{D_{II}} \int_{-D_{II}/2}^{D_{II}/2} \frac{\sinh(2\pi W/D_{II})}{\cosh(2\pi W/D_{II}) - \cos(2\pi x/D_{II})} dx = 1. \quad (A11)$$

Multiplying the absorbed flux  $N_{\text{abs}}$  of Eq. (A3) with the expression for  $f(x, W, D_{II})$  we find

$$N_f = N_D + N_{\text{abs}} \frac{N_B}{N_A + N_B} \frac{\sinh(2\pi W/D_{II})}{\cosh(2\pi W/D_{II}) - \cos(2\pi x/D_{II})}. \quad (A12)$$

The energy resolution of the present experiments is not sufficient to study single class II states, but instead the fission probability is averaged over many class II states. To make a comparison between theory and experiment we, therefore, need to calculate the fission probability averaged over a class II resonance. (In this Appendix for simplicity we ignore the summation over spin and parity, but in the comparisons shown in Sec. C it is included):

$$P_f = \frac{1}{D_{II}} \int_{-D_{II}/2}^{D_{II}/2} \frac{N_f}{N_f + N_I} dx, \quad (A13)$$

## SUMMARY OF FISSION PROBABILITY FORMULAS

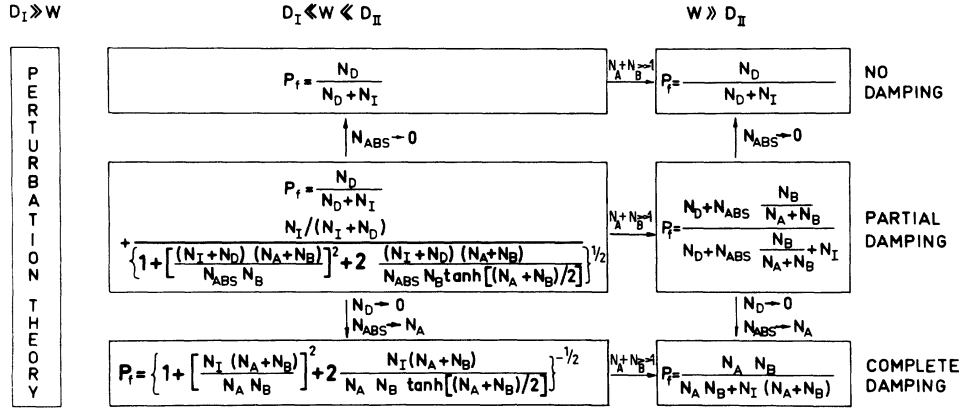


FIG. 17. A schematic representation of the formalism appropriate for calculating fission probabilities in different limits for the absorption in the second well and in different limits for the width of the compound states in the second well. Total  $K$  mixing in well II is assumed and for simplicity the summation over spin and parity has been omitted from the formulas.

where  $N_I = N + N_n$ . By substituting Eq. (A12) for  $N_f$ , we get:

$$P_f = \frac{1}{D_{II}} \int_{-D_{II}/2}^{D_{II}/2} \frac{N_D + N_{abs} [N_B / (N_A + N_B)] [\sinh(2\pi W / D_{II})] / [\cosh(2\pi W / D_{II}) - \cos(2\pi x / D_{II})] dx}{N_D + N_{abs} [N_B / (N_A + N_B)] [\sinh(2\pi W / D_{II})] / \cosh(2\pi W / D_{II}) - \cos(2\pi x / D_{II}) + N_I} \quad (A14)$$

$$= \frac{N_D}{N_D + N_I} + [N_I / (N_I + N_D)] \left/ \left( 1 + \left| \frac{(N_I + N_D)(N_A + N_B)}{N_{abs} N_B} \right|^2 + 2 \frac{(N_I + N_D)(N_A + N_B)}{N_{abs} N_B \tanh[(N_A + N_B)/2]} \right)^{1/2} \right. \quad (A15)$$

In deriving Eq. (A15) from Eq. (A14) we have made use of the assumption that the width  $W$  of the class II state stems from the escape width through the barriers  $A$  and  $B$ , and hence can be written

$$W = \frac{D_{II}}{2\pi} \frac{1}{2} (N_A + N_B). \quad (A16)$$

Now it is interesting to see what happens to this general expression for the fission probability when different extreme situations are approached. The absorbed flux  $A$  in Eq. (13) in Sec. 4 B 3 in the limit of a very strong imaginary potential in the second well is identical to the transmission coefficient one would expect if only the first barrier was present. In the same limit we find that the directly transmitted flux  $T_D$  goes to zero, and we therefore find  $N_{abs} = N_A$  and  $N_D = 0$  in this limit. In the other extreme situation, namely where there is no imaginary potential in the second well, we find  $N_{abs} = 0$ .

The effect of the coupling to the class II states

discussed in this Appendix is expected to disappear with increasing energy. This occurs when the natural width  $W$  of the class II states gets larger than the spacing  $D_{II}$  or when  $(N_A + N_B)/2 \gg 1$ . This is the limit used for the model described in Sec. 4 that was used to analyze the experimental results.

In Fig. 17 we have illustrated the form of the fission-probability expression in various situations. It is seen that the general formula of Eq. (A15) in the limit  $W \gg D_{II}$  reduces to the usually adopted formulas. However, in the limit  $W \ll D_{II}$  the present formalism will be inadequate. In this case a detailed perturbation-theory treatment as described by Lynn<sup>54</sup> should be adopted.

### C. Effect on the fits to experimental data

In Fig. 18 we show the results of calculations performed with Eq. (A15) which incorporate the

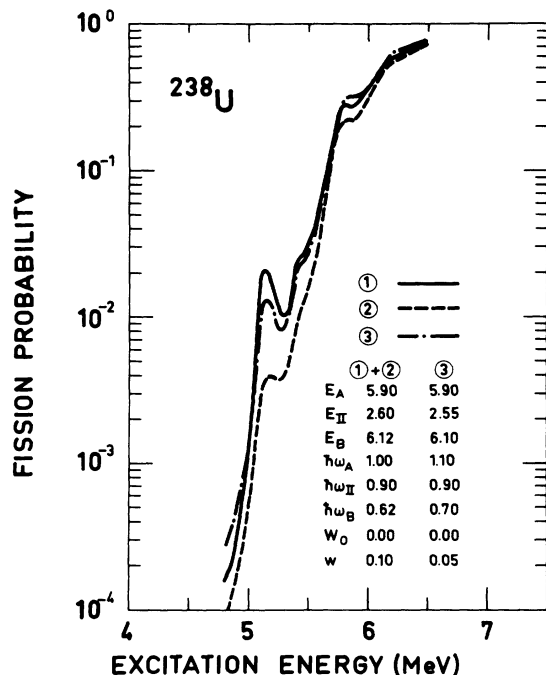


FIG. 18. Fission probabilities calculated for  $^{238}\text{U}$ . Curve 1 shows the calculation with the model used to fit experimental data except for neglect of the statistical fluctuation of the fission width. Curve 2 shows calculated results with the same parameters as used for curve 1, but with the inclusion of the coupling effects between states in well I and well II. Curve 3 employs the same model as curve 2, but the parameters have been readjusted to give a better characterization of the experimental data.

more general coupling between wells I and II, and we compare these calculations with results from the limiting case where  $W \gg D_{II}$  (see Fig. 17). Except for the neglect of the statistical fluctuations on the fission width the  $W \gg D_{II}$  limit is equivalent to the model used in the analysis of the experimental data. The results in Fig. 18 show that the inclusion of the detailed coupling between states in the two wells [Eq. (A15)] has a significant effect on the calculated fission probabilities. The result is that below 6 MeV  $P_f(E)$  shows a steeper dependence on energy and the resonances appear significantly more damped. Figure 18 also shows a calculation with Eq. (A15) where the  $\hbar\omega$  values have been increased by  $\sim 10\%$  [to decrease the slope of  $P_f(E)$ ] and the imaginary potential decreased by a factor of 2 (to restore the resonance structure). This new set of parameters with Eq. (A15) gives an equivalent fit to the experimental data and yields effectively the same values of  $E_A$  and  $E_B$ . From this comparison we conclude that the neglect of these coupling effects in the model used to extract barrier parameters from the experimental results does not affect the  $E_A$  and  $E_B$  values within the quoted errors, but the estimates of  $\hbar\omega_A$  and  $\hbar\omega_B$  (Table VI) might be too low by the order of 10%. Furthermore, we may have partially compensated for the effect of this coupling on the resonance structures by using a strength of the imaginary potential that is about twice as large as would have been found if the more general formalism of the present Appendix had been used in the analysis.

\*Work done under the auspices of the U.S. Atomic Energy Commission.

†Present address: Brookhaven National Laboratory, Upton, New York 11973.

<sup>1</sup>S. M. Polikanov, V. A. Druin, V. A. Karnaukhov, V. L. Mikheev, A. A. Pleve, N. K. Skobelev, V. G. Subbotin, G. M. Ter-Akop'jan, and V. A. Fomichev, Zh. Eksp. Teor. Fiz. **42**, 1464 (1962) [transl.: Sov. Phys. JETP **15**, 1016 (1962)].

<sup>2</sup>E. Migneco and J. P. Theobald, Nucl. Phys. **A112**, 603 (1968).

<sup>3</sup>A. Fubini, J. Blons, A. Michaudon, and D. Paya, Phys. Rev. Lett. **20**, 1373 (1968).

<sup>4</sup>N. Lark, G. Sletten, J. Pedersen, and S. Bjørnholm, Nucl. Phys. **A139**, 481 (1969).

<sup>5</sup>V. M. Strutinsky, Nucl. Phys. **A95**, 420 (1967); **A122**, 1 (1968).

<sup>6</sup>S. G. Nilsson, C. F. Tsang, A. Sobiczewski, Z. Szyman-ski, S. Wycech, C. Gustafson, I. L. Lamm, P. Möller, and B. Nilsson, Nucl. Phys. **A131**, 1 (1969).

<sup>7</sup>M. Bolsterli, E. O. Fiset, J. R. Nix, and J. L. Norton, Phys. Rev. C **5**, 1050 (1972).

<sup>8</sup>M. Brack, J. Damgaard, A. S. Jensen, H. C. Pauli, V. M. Strutinsky, and C. Y. Wong, Rev. Mod. Phys. **44**, 320 (1972).

<sup>9</sup>H. C. Pauli and T. Ledergerber, Nucl. Phys. **A175**, 545 (1971).

<sup>10</sup>U. Mosel and H. W. Schmitt, Nucl. Phys. **A165**, 73 (1971).

<sup>11</sup>J. A. Northrop, R. H. Stokes, and K. Boyer, Phys. Rev. **115**, 1277 (1959).

<sup>12</sup>H. C. Britt, F. A. Rickey, Jr., and W. S. Hall, Phys. Rev. **175**, 1525 (1968).

<sup>13</sup>J. Pederson and B. D. Kuzminov, Phys. Lett. **29B**, 176 (1969).

<sup>14</sup>B. B. Back, J. P. Bondorf, G. A. Otroschenko, J. Pedersen, and B. Rasmussen, in *Proceedings of the Second International Atomic Energy Agency Symposium on Physics and Chemistry of Fission, Vienna, 1969* (International Atomic Energy Agency, Vienna, 1969), p. 351.

<sup>15</sup>H. J. Specht, J. S. Fraser, J. C. D. Milton, and W. G. Davies, in *Proceedings of the Second International Atomic Energy Agency Symposium on Physics and Chemistry of Fission, Vienna, 1969* (see Ref. 14), p. 363.

<sup>16</sup>J. P. Bondorf, Phys. Lett. **31B**, 1 (1970).

<sup>17</sup>B. B. Back, H. C. Britt, J. D. Garrett, Ole Hansen, and B. Leroux, to be published.

<sup>18</sup>B. B. Back, H. C. Britt, J. D. Garrett, and Ole Hansen,

- Phys. Rev. Lett. 28, 1707 (1972).
- <sup>19</sup>B. B. Back, Ole Hansen, H. C. Britt, and J. D. Garrett, Phys. Lett. 46B, 183 (1973).
- <sup>20</sup>B. B. Back, Ole Hansen, H. C. Britt, and J. D. Garrett, in Proceedings of the Third International Atomic Energy Agency Symposium on Physics and Chemistry of Fission, Rochester, 1973 (to be published), paper No. IAEA-SM-174/27.
- <sup>21</sup>B. B. Back, H. C. Britt, J. D. Garrett, Ole Hansen, and B. Lewoux, in Proceedings of the Third International Atomic Energy Agency Symposium on Physics and Chemistry of Fission, Rochester, 1973 (see Ref. 20), paper No. IAEA-SM-174/201.
- <sup>22</sup>J. Saudinos, G. Vallois, O. Beer, M. Gendrot, and P. Lopato, Phys. Lett. 22, 492 (1966).
- <sup>23</sup>J. H. Bjerregaard, Ole Hansen, O. Nathan, and L. Vistisen, Nucl. Phys. A113, 484 (1968).
- <sup>24</sup>P. D. Barnes, E. R. Flynn, G. J. Igo, and D. D. Armstrong, Phys. Rev. C 1, 228 (1970).
- <sup>25</sup>C. Ellegaard and P. Vedelsby, Phys. Lett. 26B, 155 (1968).
- <sup>26</sup>N. B. Gove and A. H. Wapstra, Nucl. Data A11, 127 (1972).
- <sup>27</sup>J. D. Cramer and H. C. Britt, Phys. Rev. C 2, 2350 (1970); J. D. Cramer, Los Alamos Scientific Laboratory Report No. LA 4198, 1969 (unpublished).
- <sup>28</sup>P. D. Kunz, private communication.
- <sup>29</sup>J. D. Cramer and J. R. Nix, Phys. Rev. C 2, 1048 (1970).
- <sup>30</sup>C. Y. Wong and J. Bang, Phys. Lett. 29B, 143 (1969).
- <sup>31</sup>B. B. Back, J. P. Bondorf, G. A. Otroschenko, J. Pedersen, and B. Rasmussen, Nucl. Phys. A165, 449 (1971).
- <sup>32</sup>H. C. Britt, S. C. Burnett, and J. D. Cramer, in *Proceedings of the Second International Atomic Energy Agency Symposium on Physics and Chemistry of Fission, Vienna, 1969* (see Ref. 14), p. 375.
- <sup>33</sup>P. Möller and S. G. Nilsson, Phys. Lett. 31B, 283 (1970).
- <sup>34</sup>H. C. Pauli, T. Ledergerber, and M. Brack, Phys. Lett. 34B, 264 (1971).
- <sup>35</sup>M. G. Mustafa, U. Mosel, and H. W. Schmitt, Phys. Rev. Lett. 28, 1536 (1972).
- <sup>36</sup>P. Möller, S. G. Nilsson, and R. K. Sheline, Phys. Lett. 40B, 329 (1972).
- <sup>37</sup>S. E. Larsson, I. Ragnarsson, and S. G. Nilsson, Phys. Lett. 38B, 269 (1972).
- <sup>38</sup>U. Götz, H. C. Pauli, and K. Junker, Phys. Lett. 39B, 436 (1972).
- <sup>39</sup>D. L. Hill and J. A. Wheeler, Phys. Rev. 89, 1102 (1953).
- <sup>40</sup>H. C. Britt, S. C. Burnett, B. H. Erkkila, J. E. Lynn, and W. E. Stein, Phys. Rev. C 4, 1444 (1971).
- <sup>41</sup>A. Gilbert and A. G. W. Cameron, Can. J. Phys. 43, 1446 (1965).
- <sup>42</sup>H. C. Britt, Nucl. Data A12, 407 (1973).
- <sup>43</sup>H. C. Britt, M. Bolsterli, J. R. Nix, and J. L. Norton, Phys. Rev. C 7, 801 (1973).
- <sup>44</sup>P. Russo, J. Pedersen, and R. Vandenbosch, in Proceedings of the Third International Atomic Energy Agency Symposium on Physics and Chemistry of Fission, Rochester, 1973 (see Ref. 21), paper No. IAEA-SM-174/96.
- <sup>45</sup>B. L. Andersen, B. B. Back, and J. M. Bang, Nucl. Phys. A147, 33 (1970).
- <sup>46</sup>H. C. Pauli and T. Ledergerber, in Proceedings of the Third International Atomic Energy Agency Symposium on Physics and Chemistry of Fission, Rochester, 1973 (see Ref. 21), paper No. IAEA-SM-174/206.
- <sup>47</sup>S. Björnholm and J. E. Lynn, to be published.
- <sup>48</sup>W. D. Myers and W. J. Swiatecki, Ark. Fys. 36, 343 (1967).
- <sup>49</sup>L. G. Moretto, in Proceedings of the Third International Atomic Energy Agency Symposium on Physics and Chemistry of Fission, Rochester, 1973 (see Ref. 21), paper No. IAEA-SM-174/204.
- <sup>50</sup>P. Möller and J. R. Nix, in Proceedings of the Third International Atomic Energy Agency Symposium on Physics and Chemistry of Fission, Rochester, 1973 (see Ref. 21), paper No. IAEA-SM-174/202.
- <sup>51</sup>W. D. Myers and W. J. Swiatecki, University of California Lawrence Berkeley Laboratory Report No. LBL-1957, 1973 (to be published).
- <sup>52</sup>S. E. Larsson and G. Leander, in Proceedings of the Third International Atomic Energy Agency Symposium on Physics and Chemistry of Fission, Rochester, 1973 (see Ref. 21), paper No. IAEA-SM-174/6.
- <sup>53</sup>J. E. Lynn, private communication.
- <sup>54</sup>J. E. Lynn, in *Proceedings of the Second International Atomic Energy Agency Symposium on Physics and Chemistry of Fission, Vienna, 1969* (see Ref. 14), p. 249.